Netherlands Journal of Sea Research
27 (1): 1-23 (1990)

OBSERVATIONS ON THE HORIZONTAL AND VERTICAL STRUCTURE OF CURRENTS AT SUB-TIDAL FREQUENCIES IN THE CENTRAL NORTH SEA

J.J.M. VAN HAREN
Netherlands Institute for Sea Research, P.O. Box 59, 1790 AB Den Burg, Texel, The Netherlands

ABSTRACT

During the spring of 1986 and the summer of 1987 current, bottom pressure and CTD data were gathered in the North Sea 60 km north of the Netherlands to determine the contribution of three mechanisms to the local dynamics: wind stress, density differences and rectification due to non-linear tide-topography interaction. This was achieved by comparing the observations with simplified mathematical models each describing one of the processes.

Although a 'global' wind-driven model disagreed rather strongly with the data if the total period of measurements is considered, reasonable agreement has been obtained for small subperiods of constant wind action. During a selected period of SW-wind stress of 0.2 $N \cdot m^{-2}$, 6 ± 2 $cm \cdot s^{-1}$ of the dominating along-isobath current was wind-driven. Near the bottom above the steepest bottom slope additionally 5.5 ± 1.7 $cm \cdot s^{-1}$ was due to the frontal zone. Above this slope additionally 1.8 $cm \cdot s^{-1}$ was attributed to the rectifying mechanism. It is noted, however, that the latter value was smaller than the sum of the uncertainties in the currents resulting from the other models. The observed near-bottom along-isobath current velocity was 12.3 $cm \cdot s^{-1}$.

The density-induced motion was not explained by the thermal wind relation when integrated from the bottom upwards. The absence of sea-level adjustment and, to a lesser extent, internal friction had to be considered. At the same position the vertical shear of the cross-isobath current component generally was largest compared with other moorings due to the enhanced cross-isobath circulation by the density gradient and the rectifying mechanism.

1. INTRODUCTION

During the spring of 1986 and the summer of 1987 current meter, bottom pressure gauge and CTD data were recorded in an area of the North Sea, some 60 km north of the Dutch Frisian Islands. The area of interest, marked by the rectangle in Fig. 1, shows a diversity of transitions in the horizontal plane, both in the water column and in its bottom morphology. Hydrographically the area is marked by the transition between relatively salty (35 ppt) Channel water and less haline Central North Sea water. At times a second transition is found due to the interference of relatively fresh Coastal water (LEE, 1980). Thermal stratification parameters predict the occurrence of a tidal mixing front in this area during the summer (PINGREE & GRIFFITHS, 1978; VAN AKEN, 1986). All transition zones appear to concentrate above the steepest bottom slope ($1.2 \cdot 10^{-3}$) in the area (Fig. 2).

In comparison with other parts of the North Sea, this area is unique in that several motion-generating processes are located in a small area: the horizontal transitions in density; the transition in tidal current amplitude between strong tidal currents in the southern North Sea and moderate ones in the central North Sea; the moderately steep bottom slope, with isobaths running approximately in a straight line over a distance of 200 km; the near-coastal influence on wind-driven flows and freshwater outflow. Each of these observations may appear in stronger intensity in other parts of the North Sea, but a combination as sketched above seems not to occur anywhere, except perhaps in the German Bight.

The measurements are used to gain insight in the local dynamics of the area at sub-tidal frequencies (<0.7 cpd). Sub-tidal motions are mainly wind-driven, but contributions to their dynamics are expected from horizontal density gradients and from non-linear tidal interactions. The aim of our investigations is to determine the contribution from each of these processes to the motions observed. Two methods may be applied: spectral separation and comparison of the data with models.

Considering the (horizontal) spatial characteristics, the wind-driven motions are expected to vary over cross-isobath distances of O(Ro), with $Ro \approx 150$ km the external Rossby radius (CSANADY, 1982), as long as the sea is assumed to have a homogeneous density distribution. Density-driven motions vary over

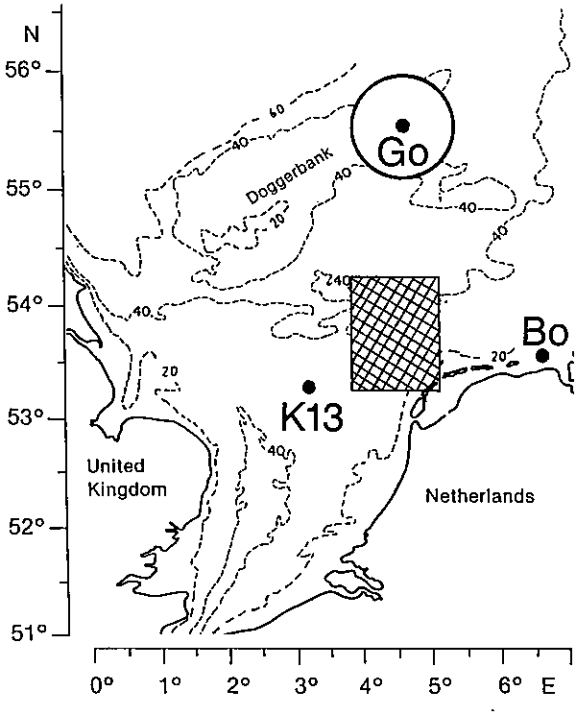

Fig. 1. Southern part of the North Sea, with the investigation area marked by the rectangle. Wind data are measured at platform K_{13}, at station Bo and in area Go.

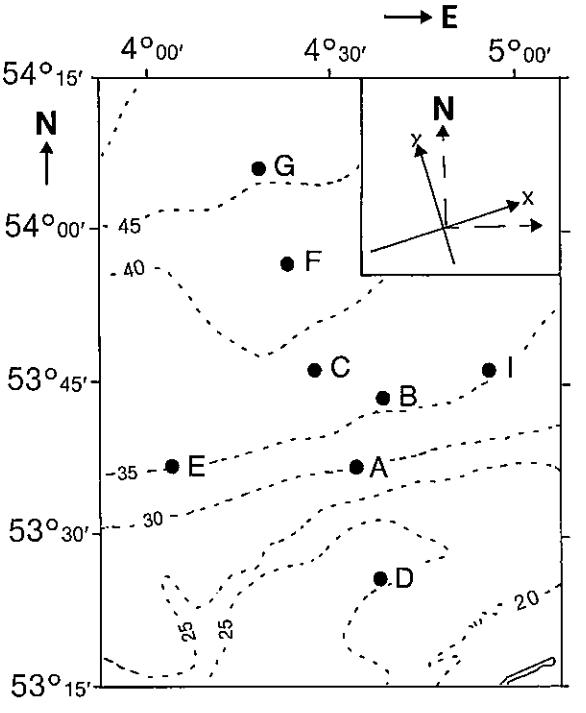

Fig. 2. Investigation area with mooring positions marked by ● and named by letters. Isobaths (dashed) are drawn every 5 m. In the upper right corner the horizontal axes of the local coordinate grid are given.

smaller scales of O(10 km) (VAN AKEN *et al.*, 1987), while non-linear tide-topography interaction produces currents varying on scales of the order of the tidal excursion length of O(1–10 km) (ZIMMERMAN, 1978; 1980; LODER, 1980; MAAS *et al.*, 1987; MAAS & ZIMMERMAN, 1989). In our area currents generated by both small-scale mechanisms seem to be located above the steepest bottom slope.

Under unstratified conditions barotropic non-linear interactions can be separated from the other mechanisms, due to their near-independence of time if averaged over a month. In a stratified sea their baroclinic equivalents are dependent on the changes in the rate of stratification, which also influences the vertical wind-induced current structure. The density-driven motions strengthen and weaken with the position and magnitude of the horizontal density gradients (fronts), which are subject to advection due to the wind-driven current.

The mutual mooring distances are O(10 km) (Fig. 2) and have been chosen to match the estimated size of frontal meanders (VAN AKEN *et al.*, 1987). However, the uncertainties in the position and width of the front *a posteriori* caused difficulties in the spectral separation of the smallest scale processes from the data. Therefore, different mathematical models, each describing the dynamical processes, have been tested against the data. A similar approach is used for instance by BUTMAN & BEARDSLEY (1987) for monthly mean data around Georges Bank.

After the presentation of the data in Section 2, the basic equations are given in Section 3. A description of the models and their comparison with the observations can be found in Section 4, followed in Section 5 by a discussion of the circulation in the vertical cross-isobath plane.

Fig. 3. Low pass filtered time series as obtained in June 1986 (left) and July 1987 (yearday 151= June 1st). a. cross-isobath current component (mooring B) in cm/s b. along-isobath current component (mooring B) in cm/s c. cross-isobath wind stress (station K_{13}) in 10^{-2} N m^{-2} d. along-isobath wind stress (station K_{13}) in 10^{-2} N m^{-2} e. vertical component of the wind stress curl per unit mass, divided by a constant waterdepth in 10^{-10} s^{-2} f. temperature difference in °C between uppermost and lowest current meters for differently labeled moorings. In (a) and (b) the solid line represents the uppermost current meter record and the dashed line the lowest.

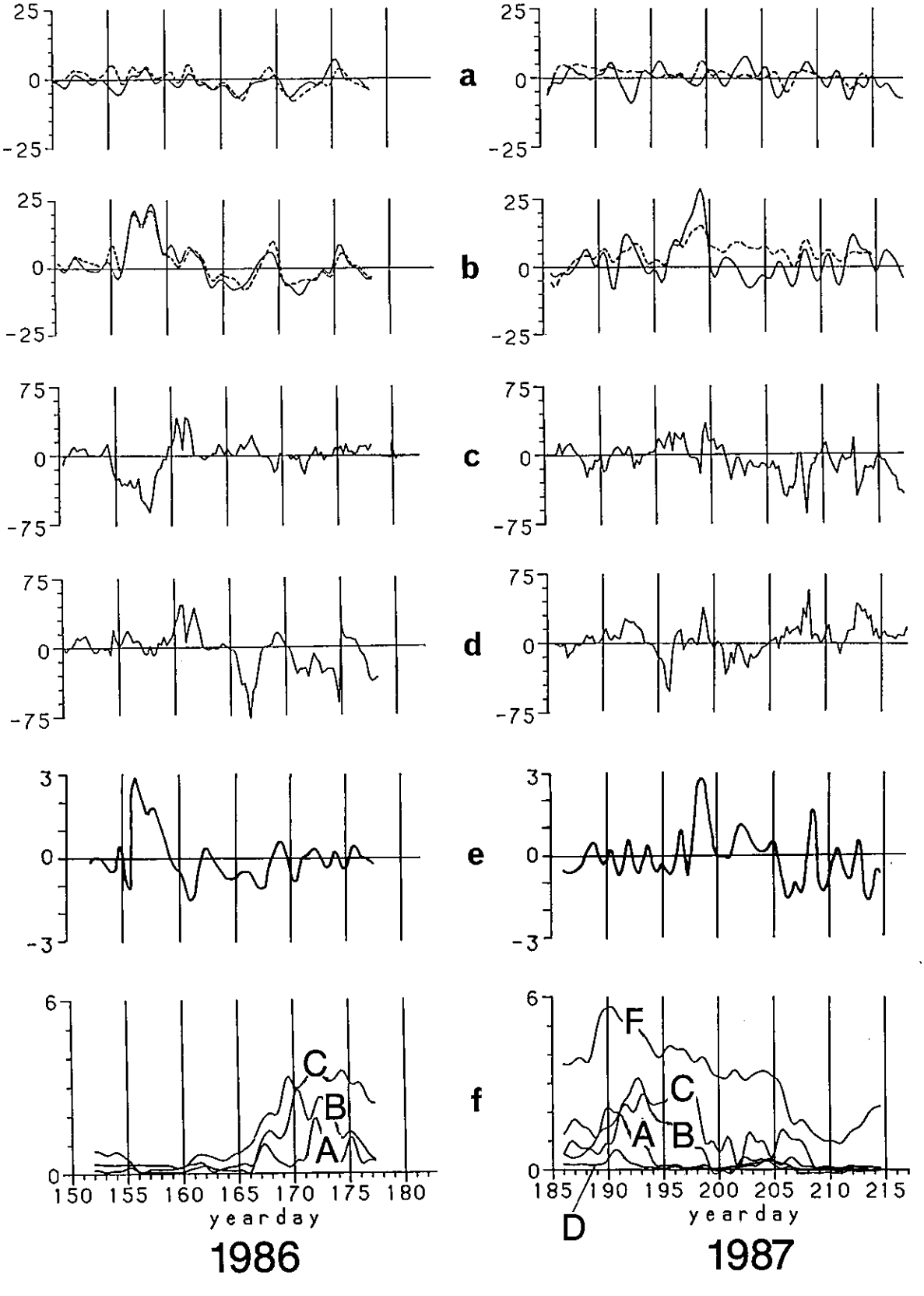
25
0
-25
a
b
75
-75
c
d
3
-3
e
6
C
B
A
150 155 160 165 170 175 180
yearday
1986
F
C
A
B
D
185 190 195 200 205 210 215
yearday
1987
f

Acknowledgements.—I wish to thank the crew of RV 'Aurelia' for the pleasant cooperation during the cruises and Kees Veth for his help in the organization of the cruises. I greatly acknowledge the 'last-minute' redrawing of some figures by Rinus Manuels. Li Honghai calculated the density-induced geostrophic flow components. Leo Maas always allowed time for stimulating discussions on the analysis and interpretations of the data. Cor Westra kindly supplied the drifter-buoy data. Part of the CTD data have been obtained on board R.V. 'Holland' and were supplied by the North Sea Division of the Dutch Ministry of Transport and Public Works. A. de Jong of T.U. Eindhoven managed to find the path to these data. I like to thank Sjef Zimmerman for his support and stimulating critisism.

The author is supported by a grant of the Netherlands Organization for Scientific Research (NWO).

2. DESCRIPTION OF THE DATA

The wind data have been measured at 6-h intervals at the stations indicated in Fig. 1. CTD-data have been obtained with a Neil Brown smart CTD on board R.V. 'Aurelia' and Guildline CTD's on board R.V. 'Tyro' and R.V. 'Holland'. The positions of the eight moorings are shown in Fig. 2. At each mooring a DAG6000 pressure gauge has been located together with two to five NBA-DNC 2M (or 2B) current meters. For technical reasons, *e.g.* wave damage, current meters have been located below 10 m from the surface. The accuracy of an individual sample was ±2.5 mb for pressure and ±1 cm·s^{-1}, ±5° TN for current speed and direction, respectively.

The x- and y-axis of the right-handed coordinate system point approximately along and perpendicular to the isobaths, respectively. The origin is located at

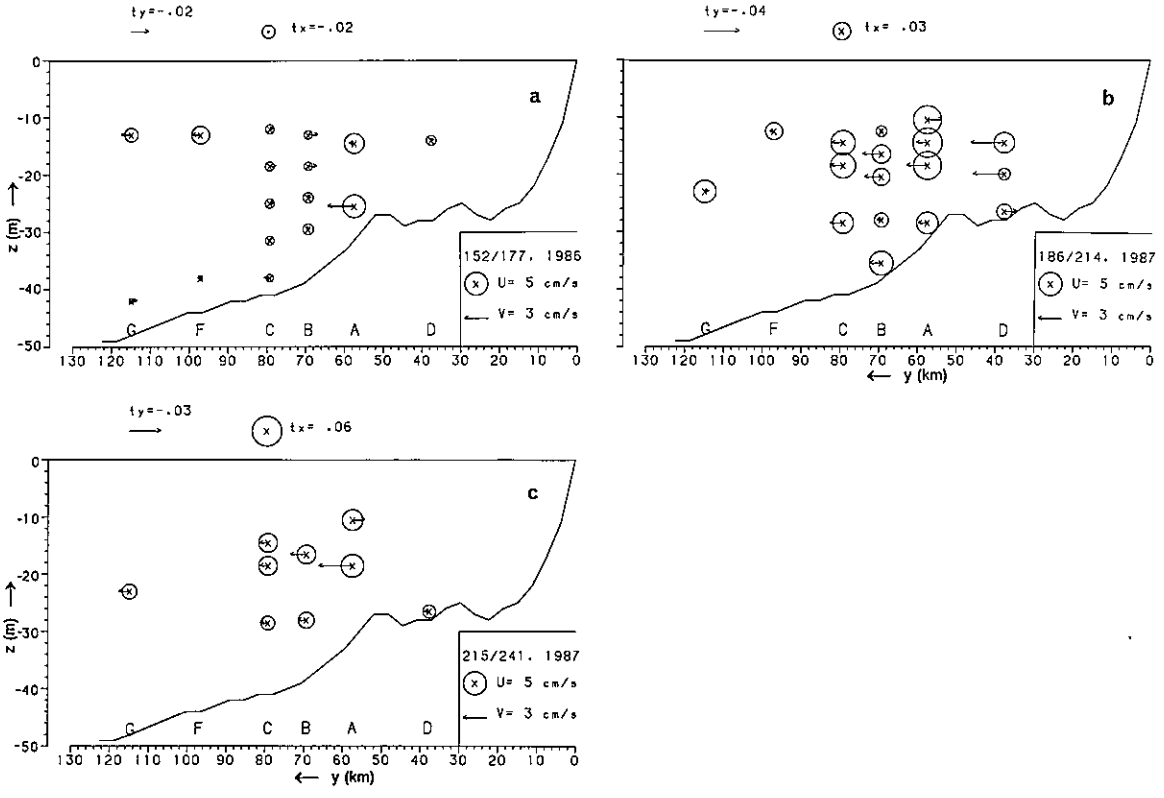

Fig. 4. Monthly averaged currents and wind stresses shown in a vertical plane along the y-axis for June 1986 (a), July 1987 (b) and August 1987 (c). The origin is located at 53°08' N and 4°45'E. Along-isobath velocities are given by circles, the radius of which is determined by their magnitudes. Crosses (dots) in the center of the circle indicate a positive, eastward (negative, westward) direction. Arrows represent the magnitude and direction of the cross-isobath currents. The scales for both current directions and the averaging period (in days) are indicated in the lower right corner. Above each figure the magnitude and direction of the average wind stress are given in N m^{-2}. The letters indicate the mooring positions.

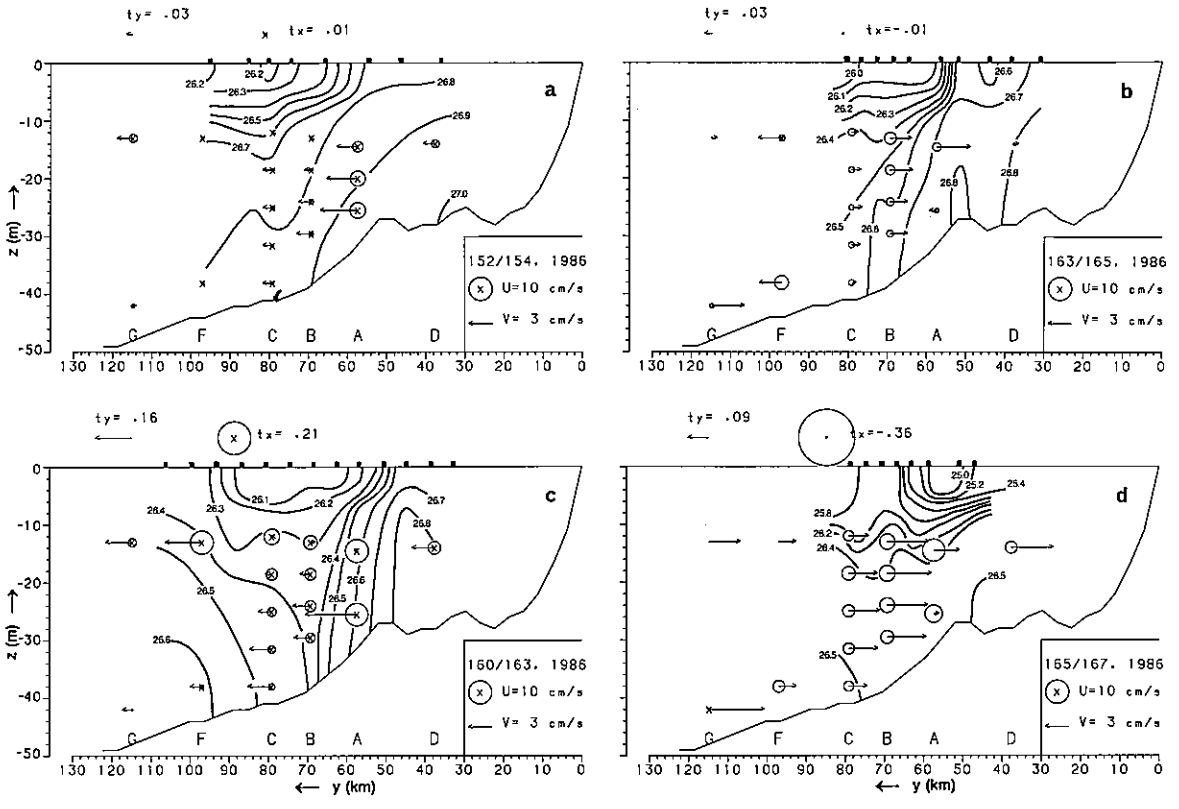

Fig. 5. Examples of currents averaged over typically 2–3 days for June 1986. The presentation is similar as in Fig. 4. Heavy solid lines represent lines of constant density excess in kg m^{-3}, interpolated from CTD measurements performed at the stations indicated by tickmarks. a. weak positive along-isobath wind stress; hydrography obtained between days 153.5–154.0 b. weak negative along-isobath wind stress; hydrography obtained between days 163.3–164.1 c. positive along-isobath wind stress; hydrography obtained between days 162.7–163.1 d. negative along-isobath wind stress; hydrography obtained between days 168.0–168.3.

the Dutch coast. Two periods will be considered specifically: June 1986 and July 1987. During the latter period nearly all moored instruments returned data, but hardly any CTD data were obtained. A description of data-acquisition and handling is given in VAN HAREN (1990), where also the data and their correlations are described. Additional information on the hydrography during June 1986 has been described by LI *et al.* (1989).

Fig. 3 shows typical time series of sub-tidal currents (u,v) measured at mooring B, wind stress components (τ_x,τ_y) calculated from wind data that were measured at station K_{13}, the vertical component of the wind stress curl and temperature differences between upper and lower current meters indicating changes in stratification rate.

Generally the along-isobath current component is larger than the cross-isobath component (Fig. 3a-b). In June 1986, from day 160 onward, the sub-tidal current varied with a dominant period of 5 days and was correlated with the along-isobath wind stress. In both months the wind stress curl varied irregularly. Between days 156-159, 1986, and 197-200, 1987 (Fig. 3e), a large wind stress curl is found, together with the largest along-isobath current component in both months.

The location of the uppermost current meter has often been found near or below the shallow pycnocline. Therefore, Fig. 3f must be viewed with caution. It cannot be used for statements on the exact amount and time-variability of the stratification. The CTD measurements obtained in June 1986 reveal a large contribution of salinity to the density stratification south of mooring B, especially during periods of easterly winds (VAN HAREN, 1990).

2.1. SUB-TIDAL CURRENT OBSERVATIONS

The long-term currents, averaged over periods of one month, are shown in Fig. 4 for the moorings in a cross-isobath vertical plane in the direction of the y-axis. The three periods differ somewhat in mean

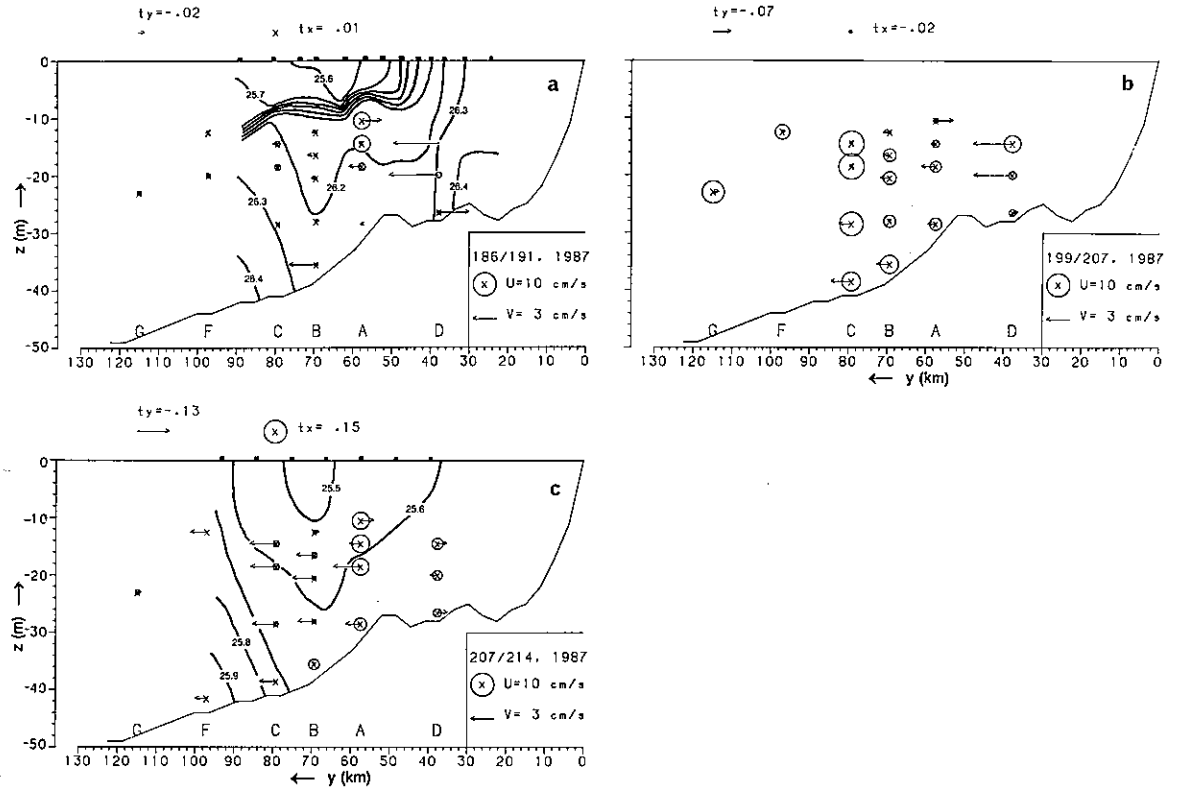

Fig. 6. Similar as Fig. 5 but for longer averaging periods of typically 5–7 days for July 1987. a. stratification offshore of mooring D; hydrography obtained between days 182.8–183.3 b. stratification offshore of mooring B (Fig. 3f); no CTD measurements c. hardly any stratification; hydrography obtained between days 210.1–210.6.

wind stress: NE-winds in June 1986 and NW-winds during the summer of 1987. The period during which the water is stratified in June 1986 and July 1987 is larger than in August 1987, when the magnitude of the along-isobath current component is nearly the same throughout the area. Irrespective of the hydrographic and wind conditions during the periods, the monthly mean along-isobath current component is always directed towards the east. It is about three times larger than the, generally offshore directed, cross-isobath component. The along-isobath current component observed at mooring A is larger by 2.9 ± 0.6 cm·s^{-1} than at the surrounding moorings B and D in June 1986 and July 1987 and by 1.4 cm·s^{-1} in August 1987.

As the mean sea level is not known for total periods of measurements of a month, no test of the momentum equations governing the monthly mean currents has been performed. The larger along-isobath currents observed at mooring A, however, cannot be attributed to a 'leak effect' (*i.e.* a residual pressure gradient) from the southern North Sea. This would generate a residual current smoothly varying over a larger cross-isobath distance than observed here.

To obtain more insight into the current amplitudes and directions during periods of different wind stresses and stratification conditions, the current components have been averaged over typically 2-5 days for selected periods (see Figs 5-6). The density distributions shown in these figures are interpolated from two cross-isobath hydrographical sections along 4°30′ and 4°40′ E, which may cause a 'positioning' error of the isopycnals of 2-4 km. They were obtained during 12 hours of measurements. In the horizontal plane the isopycnals sometimes deviate slightly (<10° from the direction of the isobaths (VAN HAREN, 1990).

In June 1986, u is larger (positive) at mooring A than at surrounding moorings except in the periods shown in Fig. 5b-d, where it is larger (negative) than at mooring D. Fig. 5a resembles Fig. 4a in the sense that $|u|_A \approx |u|_{BD} + 3$ cm·s^{-1}. The near-bottom cross-isobath current component is larger (positive) at mooring A than at B by 3.0 ± 0.1 cm·s^{-1}, causing a cross-isobath flow convergence.

During periods of dominating along-isobath winds the along-isobath current component pointed in the direction of the wind-stress, while the relatively

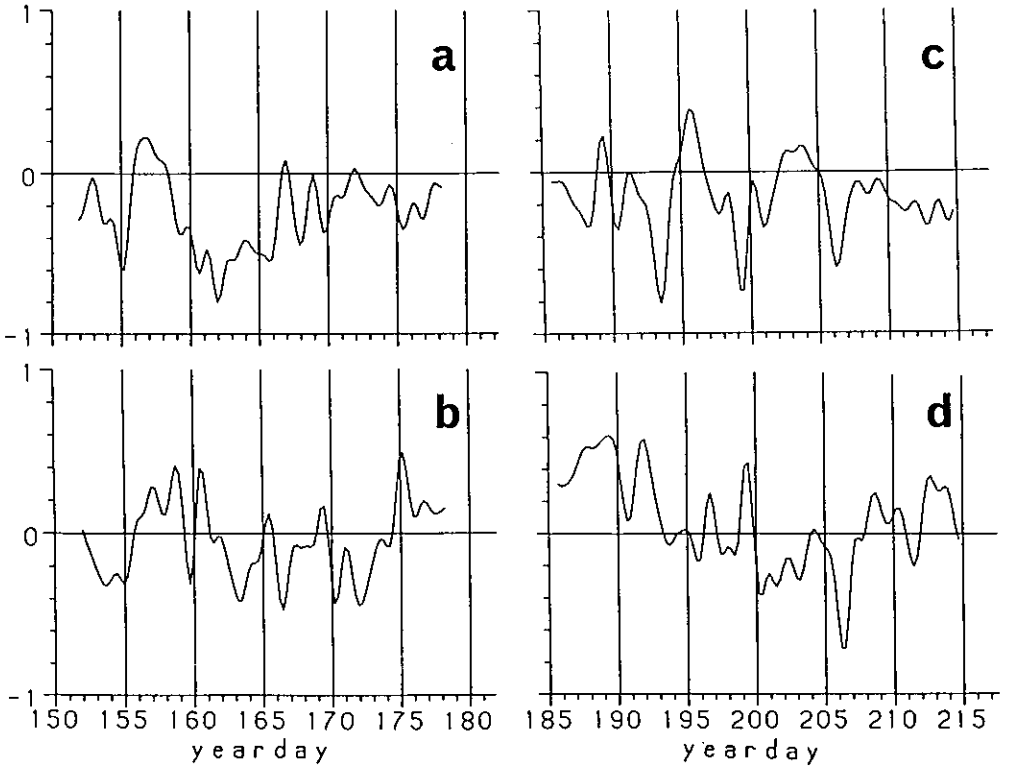

Fig. 7. Time series of vertical current shear components obtained at mooring A between the uppermost and lowest current meters. The unit of the vertical axis is $\cdot 10^{-2}$ s^{-1}. a. $\Delta v/\Delta z$, June 1986; b. $\Delta u/\Delta z$, June 1986; c. $\Delta v/\Delta z$, July 1987; d. $\Delta u/\Delta z$, July 1987.

smaller cross-isobath current component pointed to the left of u (Fig. 5c-d). This observation corresponds to the behaviour of a near-coastal region (within 1 Ro from the coast) responding to an along-isobath wind stress. The latter causes Ekman transport to the right of the wind vector in the surface layer and a cross-isobath return flow in the bottom layer (CSANADY, 1982). During both periods the most remarkable observation was again made at mooring A, where u was larger in magnitude (whether positive or negative) by 3.9 ± 1.0 cm·s^{-1} than at surrounding moorings. The observed horizontal density gradients were largest near mooring A, but they were reversed when comparing both periods. The cross-isobath near-bottom current component observed at A was larger (positive) than at B by 5.0 ± 0.4 cm·s^{-1} during both periods.

The sub-periods in July 1987 can be characterized by stratification offshore of mooring D (Fig. 6a), offshore of mooring B (Fig. 3f) and by a reduced stratification observed in the area (Fig. 6c). In comparison with the data from June 1986, the currents displayed in Fig. 6 do not show a regular pattern in the vertical or in the horizontal plane. However, again a larger (positive) along-isobath current component is observed at mooring A, except from day 199-207 when the stratification and the front moved northward (Fig. 3f).

In Sections 3 and 4 we will sort out the contributions of several mechanisms which may explain the observed currents, especially those of mooring A.

2.2. SUB-TIDAL CURRENT SHEAR OBSERVATIONS

Fig. 7 shows time series of the vertical current shear, expressed in finite differences ($\Delta u/\Delta z$,$\Delta v/\Delta z$), and calculated between the uppermost and lowest current meters at mooring A. At this mooring $\Delta v/\Delta z$ was negative during most of the time, whereas the value of $\Delta u/\Delta z$ averaged over the monthly periods was nearly zero and its time evolution was rather capricious. The magnitude of the shear components amounted to $0.7 \cdot 10^{-2}$ s^{-1}, irrespective of the current direction. Generally the amplitudes of the shear were 1–1.5 times larger between vertically consecutive current meters, with the exception of moorings D, A and B in July 1987. At these moorings the vertical current shear between the two uppermost current

meters at times reached $2 \cdot 10^{-2}$ s^{-1}.

Correlations between $\Delta u/\Delta z$, $\Delta v/\Delta z$ and other parameters such as $\Delta T/\Delta y$ (with T denoting temperature), τ_x and τ_y varied. The results from three mutually independent frequency bands (0.1, 0.31 and 0.5 cpd) showed statistically significant correlations in the two highest frequency bands only. The significantly correlating time series of the 0.31 cpd band are shown in Table 1 for moorings A, B and C. North of mooring A horizontal density gradients were mainly determined by temperature gradients and generally found in the surface layer (subscript s). In July 1987, indeed near the surface only, a coherent phase difference of approximately 180° was found between $\Delta u/\Delta z$ and $\Delta T_s/\Delta y$ as expected from the thermal wind relation (Section 4.4). It is unclear why $\Delta u/\Delta z$ at mooring A was coherent with $\Delta T_s/\Delta y$ measured between B and C. The phase difference of nearly 180° between the along-isobath wind-stress and $\Delta v/\Delta z$ at moorings B and C corresponds to wind-driven circulation in the vertical plane below the Ekman layer, as will be discussed in Sections 4 and 5.

The horizontal shear $(\partial/\partial x, \partial/\partial y)$ of both current components was calculated between consecutive moorings along both axes. The results along the x-axis gave low values (maximum amplitudes $|\Delta u/\Delta x|, |\Delta v/\Delta x| < 0.2 \cdot 10^{-5}$ s^{-1}) and are not considered further. Generally the largest shear was found in the surface layer around mooring A, *i.e.* between moorings D,A (DA) and moorings A,B (AB), with nearly similar values for the magnitudes of both current components (Figs 8 and 9). Note the persistently large negative $\Delta v/\Delta y$ between AB near the bottom in June 1986 (Fig. 8e). The variability in time was high with a general s.d. of $0.38 \pm 0.09 \cdot 10^{-5}$ s^{-1} (= $0.034 \cdot f$, where f denotes the inertial frequency) for AB,DA and a maximum amplitude of $1.0 \cdot 10^{-5}$ s^{-1}. On average, $\Delta u/\Delta y$ is negative for AB and positive for DA, *i.e.* the along-isobath current at A is larger than at its surrouding moorings. Between the other moorings and in the bottom layer the values were generally half the ones given above.

TABLE 1

Phases (in degrees) between time series, which are coherent in the 0.31 cpd band and which are calculated for the moorings A, B and C. The row leads the column in phase. If no values are shown the coherency is below the 95%-significance level. The values are for July 1987 and (between brackets) June 1986.

	$\Delta T_s/\Delta y$			
	AB	*BC*	τ_x	τ_y
$\Delta u/\Delta z$: A		165		
B	143			
C		165		(330)
$\Delta v/\Delta z$: A				
B			(170)	
C		320	(170)/190	

3. BASIC EQUATIONS

The models of the wind-driven circulation consist of finding first a solution for the vertically averaged current components, called the 'global' solution (CSANADY, 1982). This solution does not contain small-scale effects like those generated by horizontal density gradients (*cf.* Fig. 5 for their spatial scale). As a 'global' solution one may either use the vertically averaged current components as obtained by the complete equations of motion, or, one may assume the global solution to be in approximate geostrophic balance locally. In Section 4.2. we shall show that the first approach, although more correct, cannot be verified by the data, so that we have to use the second approach for a description of the local vertical structure. Then, the 'local' solution, or the vertical current structure is obtained in terms of the vertically homogeneous geostrophic current $\vec{u}_g = (u_g, v_g)$ and the Ekman solution, which accomodates for friction. The geostrophic current is calculated as

$$\vec{u}_g = \left(-\frac{1}{f\varrho}\frac{\Delta p_H}{\Delta y}, \frac{1}{f\varrho}\frac{\Delta p_H}{\Delta x}\right),$$

with p_H denoting bottom pressure fluctuations observed in areas where horizontal density gradients are small (between moorings B and F along the y-axis and B and E along the x-axis). The density-driven current is calculated from the CTD observations. Finally, those parts of the data which are unexplained by the wind-driven and density-driven circulation are compared with results from a sophisticated model of non-linear tide-topography interaction (MAAS & ZIMMERMAN, 1989).

The equations of motion along the three Cartesian coordinates in a shallow, hydrostatically balanced sea read:

$$\frac{du}{dt} - fv = -\frac{1}{\varrho}\frac{\partial p}{\partial x} + K\frac{\partial^2 u}{\partial z^2}, \tag{1a}$$

$$\frac{dv}{dt} + fu = -\frac{1}{\varrho}\frac{\partial p}{\partial y} + K\frac{\partial^2 v}{\partial z^2}, \tag{1b}$$

$$0 = -\frac{1}{\varrho}\frac{\partial p}{\partial z} - g, \tag{1c}$$

and the continuity equation:

$$0 = \frac{\partial u}{\partial x} + \frac{\partial v}{\partial y} + \frac{\partial w}{\partial z}, \tag{1d}$$

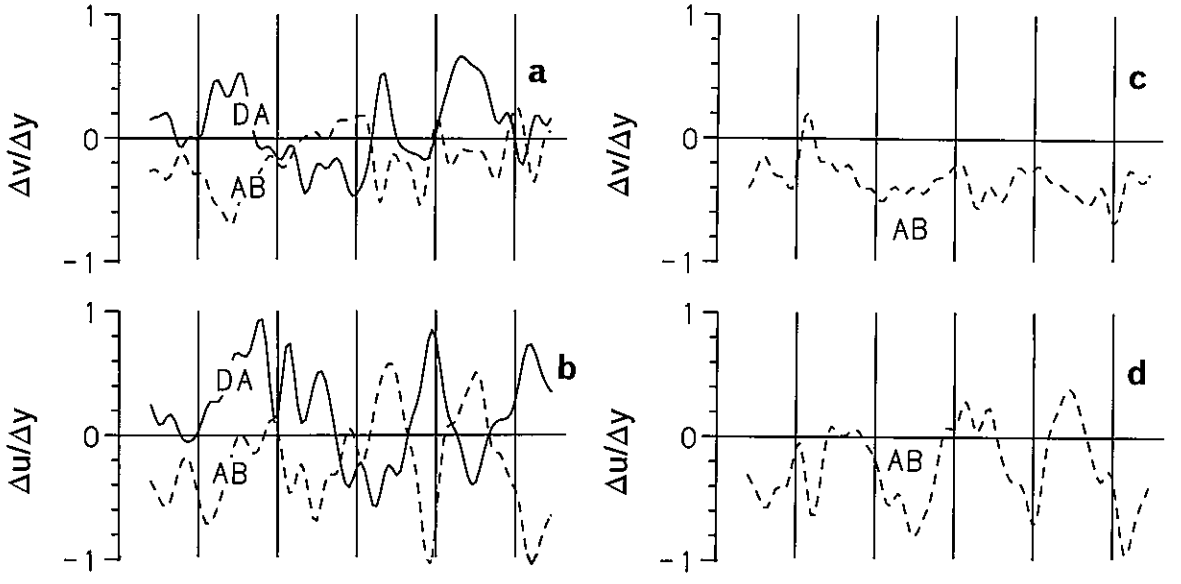

Fig. 8. Time series of the cross-isobath horizontal shear components of u and v obtained between several moorings (indicated by double letter-names) at 14 m depth (a-b) and at 8 m from the bottom (c-d) in June 1986. The unit of the vertical axis is 10^{-5} s^{-1}.

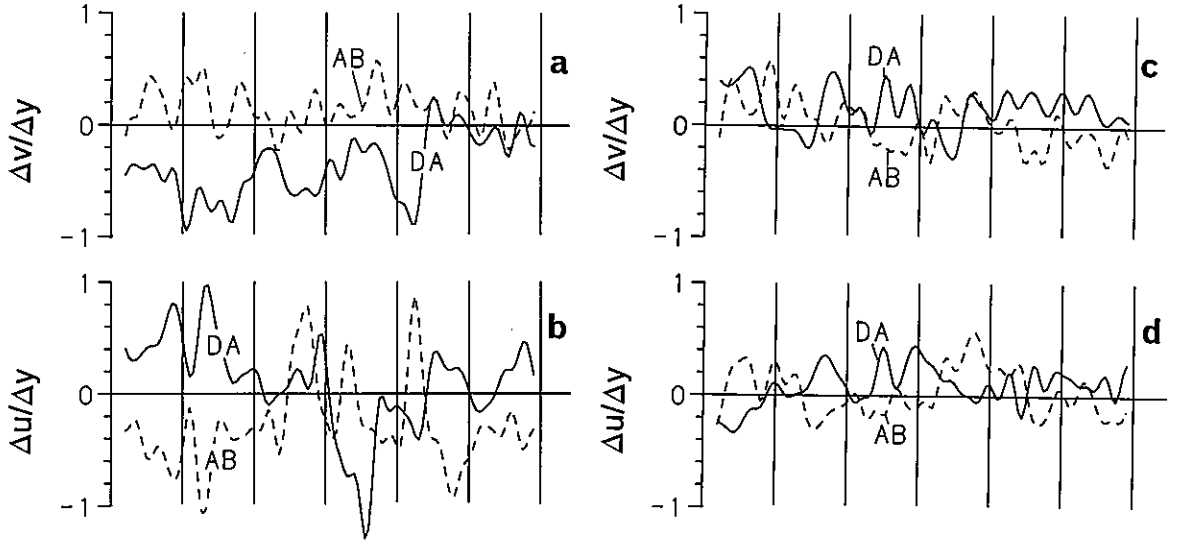

Fig. 9. Similar as Fig. 8 but for July 1987.

in which p denotes the pressure, ϱ the density, g=9.81 m s^{-2} the acceleration of gravity, f=1.175·10^{-4} s^{-1} the inertial frequency at 53°40′ N, w the vertical velocity component and K a constant vertical eddy viscosity. In the momentum equations horizontal eddy viscosity and terms containing w are neglected.

3.1. GLOBAL SOLUTIONS

Vertically and tidally averaging (1) results in the equations governing the 'global' sub-tidal transport and sea-level fluctuations. According to the data of VAN HAREN (1990) the averaged horizontal momentum equations can be approximated for areas with small horizontal density gradients as:

$$\frac{\partial <U>}{\partial t} - f<V> = -\frac{1}{\varrho}\frac{\partial <P_H>}{\partial x} + \frac{s<\tau_x>}{\varrho H} - \frac{\alpha r <U>}{H}, \qquad (2a)$$

A B B B A

$$f<U> = -\frac{1}{\varrho}\frac{\partial <P_H>}{\partial y} + \frac{s<\tau_y>}{\varrho H}, \qquad (2b)$$

C C B

to which the continuity equation is added:

$$\frac{\partial <\zeta>}{\partial t} + \frac{\partial <U>H}{\partial x} + \frac{\partial <V>H}{\partial y} = 0\,, \qquad (2c)$$

in which:

$$U = 1/(H+\zeta)\int_{-H}^{\zeta} u\,dz; \quad \text{V similar, vertically}$$

averaged current components
$< >$ = tidally averaging operator
ζ = sea-level variation
p_H = as defined before
H = water depth
α = 0.55, relating $\vec{u}_b$, the current at 1 m from the bottom, to the vertically averaged current: $|\vec{u}_b| \approx \alpha |\vec{U}|$ (MAAS & VAN HAREN, 1987)
s = 1.07, wind transport correction factor (VAN HAREN, 1990).

The bottom friction has been parametrized by a linear stress law. The parameter r is chosen constant in space and time as $r = 1.0 \cdot 10^{-3}$ m s^{-1} (BOWDEN, 1953; NOBLE *et al.*, 1983). This value is larger than observed for tidal currents by MAAS & VAN HAREN (1987) ($0.29 \cdot 10^{-3}$ m s^{-1}) and lower than the value adopted by WEENINK (1958) in his model on wind-driven currents ($4.4 \cdot 10^{-3}$ m s^{-1}).

The terms in (2a) and (2b) are approximately in the ratio of A:B:C $\approx$ 1:3:8 ($\cdot 0.075 \cdot 10^{-5}$ m s^{-2}). Note the approximate geostrophic balance in the cross-isobath direction (VAN HAREN, 1990). It is impossible to find a proper balance of (2c) by using the data, which is probably due to large uncertainties in the vertically averaged current components and their spatial derivatives (Section 4). For motions at subtidal frequencies, however, we may adopt a rigid lid approximation for which the first term in (2c) can be neglected.

The generation processes of the tidally and vertically averaged wind-driven circulation are more transparent in the vorticity equation, which is obtained by taking the curl of (2a) and (2b). With a rigid lid approximation (2c) allows for the introduction of a stream (actually 'transport') function $\Psi(x,y,t)$, defined as: $\partial\Psi/\partial y = -UH$; $\partial\Psi/\partial x = VH$. After dropping the tidally averaging operator and with $\partial H/\partial x << \partial H/\partial y$ as applies to the area concerned, the vorticity equation reads:

$$\frac{\partial^2}{\partial t \partial y}\left(\frac{1}{H}\frac{\partial \Psi}{\partial y}\right) - \frac{f}{H^2}\frac{\partial H}{\partial y}\frac{\partial \Psi}{\partial x} + \alpha r \frac{\partial}{\partial y}\left(\frac{1}{H^2}\frac{\partial \Psi}{\partial y}\right) =$$

$$= \frac{s}{\varrho H}\vec{k}\cdot(\vec{\nabla}\times\vec{\tau}) + \frac{s\tau_x}{\varrho H^2}\frac{\partial H}{\partial y}\,, \qquad (3)$$

in which $\vec{k}$ denotes the vertical component of the unit vector.

The right-hand side (r.h.s.) of (3) expresses the vorticity generation mechanisms due to the curl of the wind stress and the bottom slope/along-isobath wind stress effect (WEENINK, 1958). The second term on the left-hand side (l.h.s.) is the planetary vortex stretching or 'topographic' vorticity term (SIMONS, 1980).

Equation (3) does not include terms with horizontal density gradients and is thus appropriate for the description of the 'global' solution. Formally, *i.e.* with p in (2) instead of the restricted $p_{,H}$, in areas with a sloping bottom the vorticity equation (3) shows an extra term proportional to $J(\varrho,H) = \partial\varrho/\partial x \cdot \partial H/\partial y - \partial\varrho/\partial y \cdot \partial H/\partial x$. In our area isopycnals run approximately parallel to the isobaths (VAN HAREN, 1990) and thus $J(\varrho,H) \approx 0$, so that (3) is valid, even when horizontal density gradients are considered.

WEENINK (1958) uses a steady state version of (3) to model the wind-driven circulation in the North Sea. Here we retain the first term in (3) to allow time for a disturbance to establish a steady current. Then, after assuming every single wind value as a single disturbance, the solution of (3) may be used to generate a time series of vertically averaged currents based on the time series of wind stress. The solution of (3) is separated in three parts: $\Psi = \Psi_1 + \Psi_2 + \Psi_3$, of which Ψ_1 is the solution with only the curl of the wind stress term retained in the r.h.s., Ψ_2 with only the second (bottom slope) term in the r.h.s. and Ψ_3 the solution when the r.h.s. is equal to zero and all forcing is at the boundaries only ('leak effect'). The boundary condition at the coast bordering the North Sea is:

$$\Psi = \Psi_1 = \Psi_2 = \Psi_3 = 0 \qquad (4)$$

The wind condition $\Psi_3 = 0$ at both the British and the Continental coasts implies that the leak effect through the Channel is considered equal to zero. As

no information on the amount of leak is available (via pressure gradients) or on its generating mechanism (like wind stress in the Channel), this condition is necessary. No serious problems are expected as comparison between model and observations will directly show a possibly missing constant current.

WEENINK (1958) assumes that the sea level and equivalently its gradient are equal to zero along the open (northern) boundary $y=L$ between the North Sea and the Atlantic Ocean, across which the water-depth rapidly increases to a large value. This condition implies that the solution of (3) entirely depends on the wind field over the North Sea itself and not on wind effects over other areas such as the Atlantic Ocean. Casting the x-momentum equation (2a) in terms of Ψ, the boundary condition at $y=L$ reads:

$$\frac{\partial^2\Psi_i}{\partial t\partial y}+\frac{\alpha\cdot r}{H^2(L)}\frac{\partial\Psi_i}{\partial y}+\frac{f}{H(L)}\frac{\partial\Psi_i}{\partial x}=0 \quad \text{for} \quad i=1 \quad \text{and} \quad 3$$

$$\frac{\partial^2\Psi_2}{\partial t\partial y}+\frac{\alpha\cdot r}{H^2(L)}\frac{\partial\Psi_2}{\partial y}+\frac{f}{H(L)}\frac{\partial\Psi_2}{\partial x}+\frac{s\tau_x}{\varrho H(L)}=0 \qquad (5)$$

WEENINK (1958) has shown that (3) with the conditions (4) and (5) can be solved analytically for specific depth profiles only. His numerical solutions for arbitrary depth profiles show, however, that our area is near the symmetry axis of the basin and of the solutions. Thus locally (in this case, say the measurement area in Fig. 1) $\partial\Psi/\partial x \rightarrow 0$. From the data it is not evident that the second term on the l.h.s. of (3) is small, but we anticipate here the results of Section 4.3.

The North Sea basin is divided in two parts. The wind-stress curl is assumed to be homogeneous for the southern region. As all periods of observed large curl of the wind stress are marked by the passage of an atmospheric low pressure area over the southern region, the contribution of the northern region is effectively neglected by assuming $\vec{k}\cdot<\vec{\nabla}x\vec{\tau}>=0$ for $y>L$, in which L is an adjustable distance offshore with a maximum value of $L_m=315$ km, the northern edge of the Dogger Bank.

Both assumptions are used to compile an approximate analytical solution of the along-isobath current velocity as a function of the cross-isobath coordinate and time:

$$\frac{-1}{H}\frac{\partial\Psi}{\partial y}=U(y,t)=\frac{Hs}{r'\varrho}\,(1-e^{-r'/Ht})\cdot$$

$$\cdot\left[\int_y^L \vec{k}\cdot<\vec{\nabla}\times\vec{\tau}>/H\,dy+\frac{\tau_x}{H}\right], \qquad (6)$$

in which $r'=\alpha r$ and the leak effect is neglected. Solution (6) shows a constant contribution of the along-isobath wind stress to the along-isobath current component throughout the area and a contribution due to the curl of the wind stress, dependent on the (integrated) depth north of the y-position under investigation. We shall test the result (6) against the data in Section 4.2.

3.2. VERTICAL CURRENT STRUCTURE; LOCAL SOLUTION OF THE WIND-DRIVEN CIRCULATION

In this section local effects on the vertical current structure due to density stratification and wind will be considered, whereas in Section 3.3 effects due to horizontal density gradients will be described. Spatial variations in density, which are important in both sections, are obtained from CTD observations, which cannot be cast in a time series. Thus, in the following sections only steady-state solutions will be considered, which will be compared in Section 4 with observations from periods of limited temporal extent (1-3 days) with quasi-stationary currents and wind.

In order to obtain the vertical structure of the local wind-driven circulation, the steady Ekman solution of (1a) and (1b) is derived for a three-layer model, comparable to the one used by MAAS & VAN HAREN (1987). The model describes a wind-mixed surface- and a tidally-mixed bottom layer, with a stratified layer of finite width in between. In complex notation the equations to be solved read (where W should not be confused with the former introduction of the vertical velocity component):

$$-fW_n=-fW_g+iK_n\frac{\partial^2W_n}{\partial z^2} \qquad n=1,2,3 \qquad (7)$$

with $W_g=u_g+iv_g$, $W_n=u_n+iv_n$ the total current (containing W_g and the frictional part), $i=\sqrt{-1}$ and with the boundary conditions:

$$K_1\frac{\partial W_1}{\partial z}=\frac{T}{\varrho} \qquad \text{with } T=\tau_x+i\tau_y \qquad \text{at } z=0,$$

$$K_1\frac{\partial W_1}{\partial z}=K_2\frac{\partial W_2}{\partial z}; \qquad W_1=W_2 \qquad \text{at } z=-h_1,$$

$$K_2\frac{\partial W_2}{\partial z}=K_3\frac{\partial W_3}{\partial z}; \qquad W_2=W_3 \qquad \text{at } z=-h_2,$$

$$K_3\frac{\partial W_3}{\partial z}=rW_3 \qquad \text{at } z=-h_3=-H.$$

The vertical eddy viscosities K_n are taken constant for each layer. The layer-depths h_n are independently adjustable. In terms of the Ekman depths $E_n=(2K_n/f)^{0.5}/(1+i)$ the solution of (7) reads:

$$W_1=2B_1\cosh(z/E_1)+\frac{T}{\varrho}\frac{E_1}{K_1}\exp(z/E_1)+W_g \qquad \text{for } -h_1<z<0$$

$$W_2=A_2\exp(z/E_2)+B_2\exp(-z/E_2)+W_g \qquad \text{for } -h_2<z<-h_1$$

$$W_3=A_3\exp(z/E_3)+B_3\exp(-z/E_3)+W_g \qquad \text{for } -h_3<z<-h_2 \qquad (8)$$

with, after defining $\gamma = h_1/E_1$:

$$B_1=[A_2\exp(-h_1/E_2)+B_2\exp(h_1/E_2)-\frac{TE_1}{\varrho K_1}\exp(-\gamma)]\ /\ 2\cosh\gamma$$

$$A_2=\frac{[B_2\exp(h_1/E_2)\,(\frac{K_2E_1}{K_1E_2}\cosh\gamma-\sinh\gamma)+\frac{TE_1}{\varrho K_1}]}{[\sinh\gamma+\frac{K_2E_1}{K_1E_2}\cosh\gamma]}$$

$$B_2=[\frac{TE_1}{\varrho K_1}\exp(h_1/E_2)\,\{(\frac{K_2}{E_2}-r)\cosh(\frac{h_3-h_2}{E_3})-(\frac{K_3}{E_3}-r\frac{K_2E_3}{K_3E_2})\sinh(\frac{h_3-h_2}{E_3})\}-$$

$$-rW_g(\frac{K_3}{E_3}-r)^{-1}\exp(\frac{h_2}{E_2}+\frac{h_3}{E_3})\,\{\frac{K_2E_1}{K_1E_2}\cosh\gamma+\sinh\gamma\}]\ /\ A_1$$

$$A_3=[B_3(\frac{K_3}{E_3}+r)\,(\exp(2h_3/E_3)+rW_g\exp(h_3/E_3)]/[\frac{K_3}{E_3}-r]$$

$$B_3=[(\frac{K_3}{E_3}-r)\{A_2\exp(-h_2/E_2)+B_2\exp(h_2/E_2)\}\exp(-h_3/E_3)-rW_g\exp(-h_2/E_3)]\ /\ [2\{\frac{K_3}{E_3}\cosh(\frac{h_3-h_2}{E_3})+r\cdot\sinh(\frac{h_3-h_2}{E_3})\}]$$

$$A_1=\exp(2h_2/E_2)\{\sinh\gamma+\frac{K_2E_1}{K_1E_2}\cosh\gamma\}\,\{(\frac{K_2}{E_2}+r)\sinh(\frac{h_3-h_2}{E_3})+(\frac{K_3}{E_3}+r\frac{K_2E_3}{K_3E_2})\cosh(\frac{h_3-h_2}{E_3})\}+$$

$$+\exp(2h_1/E_2)\{\sinh\gamma-\frac{K_2E_1}{K_1E_2}\cosh\gamma\}\,\{(\frac{K_2}{E_2}-r)\cosh(\frac{h_3-h_2}{E_3})-(\frac{K_3}{E_3}-r\frac{K_2E_3}{K_3E_2})\sinh(\frac{h_3-h_2}{E_3})\}$$

The surface-layer eddy viscosity, K_1, is taken proportional to the wind stress magnitude according to POND & PICKARD (1986):

$$K_1 = \frac{f}{2\varrho_a \sin\phi}\left(\frac{4.3}{\pi}\right)^2 |\vec{\tau}| / C_d \qquad (9)$$

in which $\varrho_a = 1.26$ kg m^{-3} denotes the density of air and ϕ the latitude. For $|\vec{\tau}| = 0.2$ N m^{-2} and a constant drag coefficient $C_d = 2 \cdot 10^{-3}$, a value of $K_1 = 11 \cdot 10^{-3}$ m^{2}s^{-1} is found. For the bottom layer eddy viscosity CSANADY (1982) gives two empirical formulations for homogeneous seas:

$$K_3^{(1)} = u_* \cdot H/16 \qquad \text{for } \frac{fH}{u_*} \to 0$$

$$K_3^{(2)} = \frac{{u_*}^2}{200f} \qquad \text{for } \frac{fH}{u_*} \to \infty \qquad (10)$$

with $u_* \approx (\alpha r |\vec{U}|)^{0.5}$ and a transition value of $fH/u_* = 0.08$ between the two limits. With the constant values $|\vec{U}| = 0.25$ m s^{-1} and $H = 35$ m we find $fH/u_* = 0.36$ and *de facto* the deep water limit $K_3^{(2)}$ has to be taken: $K_3^{(2)} \approx 5.8 \cdot 10^{-3}$ m^2 s^{-1}. As will be shown, the shallow water limit may be used under stratified conditions: $K_3^{(1)} \approx 25 \cdot 10^{-3}$ m^2 s^{-1}. The value of K_2 is kept variable. The solution (8) is tested against observations in Section 4.3.

3.3. VERTICAL CURRENT STRUCTURE; LOCAL SOLUTION OF THE DENSITY CIRCULATION

A representation of the currents induced by horizontal density gradients is obtained by calculating a steady-state solution of (1) for a given density field without stratification (BOWDEN, 1983). This approach of considering a vertical front only seems to be justified in viewing the observed fronts (Fig. 5). Although formally not correct, we here assume that inside a front vertical mixing has the same properties as on the well-mixed of the front, *i.e.* K is constant throughout the water column. However, we allow for the horizontal density gradient to be a function of z. Thus, effects on the vertical current structure by vertically varying horizontal density gradients are initially considered more important than stratification effects. Wind forcing is optional.

Assuming $\zeta/H << 1$, the equation to be solved reads in complex notation ($W = u + iv$; $W_g = u_g + iv_g$; $R = g/\varrho f \cdot (\partial\varrho/\partial y - i\partial\varrho/\partial x)$; $T = \tau_x + i\tau_y$):

$$fW = fW_g - \int_z^0 R\, dz - iK\frac{\partial^2 W}{\partial z^2} \qquad (11)$$

with boundary conditions:

$$K\frac{\partial W}{\partial z} = T \qquad \text{at } z = 0$$

$$K\frac{\partial W}{\partial z} = rW \qquad \text{at } z = -H$$

The solution is:

$$W(z) = W_g + W_a(z) + W_b(z) + W_T(z)\ , \qquad (12)$$

with: $W_a(z) = -\int_z^0 R\, dz$;

$$W_b(z) = \frac{\cosh\mu z \cdot [-r(W_g + W_a(-H)) + K(\gamma - \beta e^{\mu H}) - r\frac{\beta}{\mu}e^{\mu H}]}{\mu K \cdot \sinh\mu H + r \cdot \cosh\mu H} + \frac{\beta}{\mu}e^{-\mu z}\ ;$$

$$W_T(z) = \frac{T}{\varrho\mu K}\left(-e^{-\mu z} + \frac{\cosh\mu z \cdot (\mu K + r)e^{\mu H}}{\mu K \cdot \sinh\mu H + r \cdot \cosh\mu H}\right)\ ;$$

$$\mu = (1+i) \cdot (2K/f)^{-0.5}\ ;\ \beta = -R\,|_{z=0}\ ;\ \gamma = -R\,|_{z=-H}\ ,$$

in which $W_T(z)$ denotes the wind-driven part of the solution. This wind-driven solution is similar to (8) when in the latter the eddy viscosities of the separate layers are equal to K_3. A simpler solution of (11) is derived by considering negligible internal friction ($K \to 0$). Then, the boundary conditions given above are not valid any more and a solution exists relative to a certain level at which the total current is known:

$$W(z) = W_g - \int_z^0 R\, dz\ . \qquad (13)$$

which is the integrated 'thermal wind' relation.

In deep oceans a level of no (density-induced) motion is defined as the layer at which the levels of constant density and pressure coincide, but in shallow seas such a level is often not present, because the isopycnals extend from the surface towards the bottom. In studies of shallow seas, generally the bottom is taken as reference: $W = 0$ at $z = -H$, according to which (13) is rewritten:

$$W(z) = \int_{-H}^z R\, dz\ . \qquad (14)$$

This second, integrated version of the thermal wind relation indicates a complete balance of the density- and sea-level-induced pressures at $z=-H$. Together with (12) and (13) it will be compared with observations at mooring A in Section 4.4.

4. COMPARISON OF MODELS WITH DATA

If we define as A_n and B_n discretely sampled time series which are to be mutually compared, *e.g.* as A_n time series of observed variables and as B_n the time series resulting from a model with input from observed data of forcing etc., the difference series are:

$$C_n = A_n - B_n \,, \qquad \text{for } n=1, \ldots, N \qquad (15)$$

with N the number of samples. The degree of correspondence between A_n and B_n is derived by calculating the standard deviation (s.d.) of each series:

$$s.d._x = [\frac{1}{N} \sum_{n=1}^{N} (X_n - \overline{X})^2]^{0.5} \,, \qquad (16)$$

with X=A, B or C and $\overline{X}$ denotes the time mean. Hereafter C_n will be called 'error' series and $s.d._c$ the 'error' s.d.

The accuracy of an individual sub-tidal data point is 25 Pa (0.25 mb) for the pressure data and negligible (<0.1 cm·s^{-1}) for the current data (VAN HAREN, 1990). Before comparing the models with the data, the errors in the determination of the vertically averaged current components are considered.

4.1. ERRORS IN THE VERTICALLY AVERAGED CURRENT

The unsampled 10 m of the water column will remain an unknown, but probably most important, factor in the determination of the vertically averaged current components. As the number and positions of the current meters are different at different moorings, a vertically averaged current, to be calculated similarly for every mooring, is defined as the current at $z=-0.5{\cdot}H$; time series of this averaged current are defined as B_n. The current components thus obtained are compared with time series A_n of the vertically averaged current components based on 5 current meter data records, which are considered a somewhat more reliable estimate of the vertically averaged current (see also remarks on this in Section 4.3).

This comparison is made by using data from the moorings C(1986) and B(1987) (Table 2 and Fig. 10). Good agreement is found between the two differently determined vertically averaged time series for the along-isobath component, but the cross-isobath component shows less agreement, which is clearly expressed in Table 2.

TABLE 2

Comparison of the determination of the vertically averaged current components *U* and *V* by: a. weighed averaging over 5 current meters, b. interpolation to the level $z=-0.5{\cdot}H$. Given are the s.d. of the time series and (between brackets) their overall time mean. The unit is cm·s^{-1}.

	C 1986		*B 1987*	
	U	*V*	*U*	*V*
a:	6.3(1.9)	2.2(-0.1)	6.6(3.3)	2.0(1.1)
b:	6.7(2.0)	2.9(-0.6)	7.2(3.8)	3.1(2.3)
'error':	1.1	1.4	1.8	2.2

The average 'error s.d.'s' ($s.d._c$) of the comparison of A_n with B_n for each current component are: *U* (1.4 cm·s^{-1}) and *V* (1.8 cm·s^{-1}). With these values a minimum uncertainty ($s.d._{co}$) in the Coriolis term in (2a) is calculated: $0.21{\cdot}10^{-5}$ m^{2}s^{-1}, and in (2b): $0.16{\cdot}10^{-5}$ m^2 s^{-1}. VAN HAREN (1990) finds for the s.d.'s of the time series D_n, which result after calculating the sum of all terms in (2a) and (2b): $s.d._D = 0.30{\cdot}10^{-5}$ m s^{-2} and $0.34{\cdot}10^{-5}$ m s^{-2}, respectively.

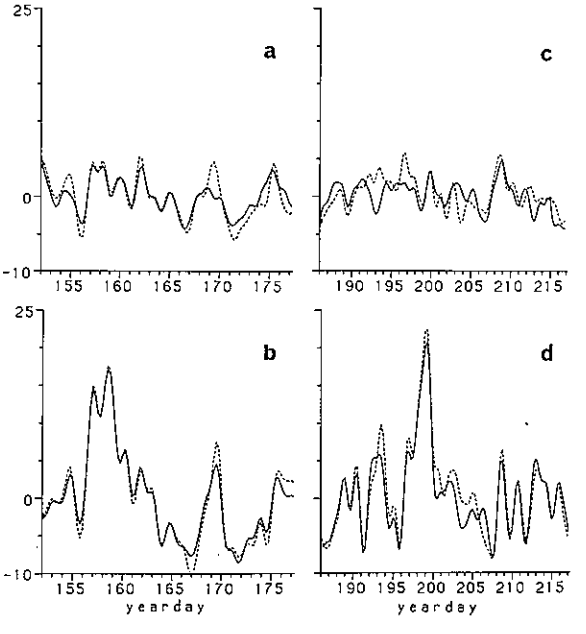

Fig. 10. Comparison of the determination of the vertically averaged current components by: (solid lines) weighted averaging over 5 current meters and (dashed lines) weighted interpolation to the level $z=-0.5{\cdot}H$. The unit of the vertical axis is cm·s^{-1}. a,b. mooring C in June 1986 c,d. mooring B in July 1987.

TABLE 3

Comparison between observed time series of along-isobath current components measured at moorings A and B (mid-depth) (s.d.$_o$) with model (6) in terms of 'error s.d.'s' (s.d.$_e$). Several best-fit parameters are given; calculations have been made for the periods June 1986 (1986_t), days 152-160 1986 (1986_p), July/August 1987 (1987_t) and days 235-247 1987 (1987_p). The unit of the s.d.'s is cm·s^{-1}, of $r \cdot 10^{-3}$ m s^{-1}. The configurations displayed in Fig. 11 are indicated. 'in/ex Dog' means in- or excluding Doggerbank.

period	*mooring*	*r*	*t*	*in/ex Dog*	*Fig. 11*	*s.d.$_o$*	*s.d.$_e$*
1986_t	B	1.0	6 hrs	ex		7.14	7.46
1986_t	B	5.0	30 hrs	in	a	7.14	5.03
1986_p	B	3.0	30 hrs	in		10.74	5.25
1987_t	B	1.0	6 hrs	ex	b	7.19	5.54
1987_t	A	1.5	6 hrs	ex	c	8.22	6.06
1987_p	B	2.0	6 hrs	in		12.06	7.02

The s.d.$_D$'s are interpreted as 'error s.d.'s' of the momentum equations. Comparing s.d.$_{co}$ with s.d.$_D$ shows that a considerable amount of D_η may be attributed to the poorly determined Coriolis terms, *i.e.* the vertically averaged current.

Attributing the remaining part of s.d.$_D$ to uncertainties in the determination of the pressure gradient, the maximum uncertainty in the geostrophic current, obtained from pressure records, then reads: $u_g(\pm 2$ cm·s$^{-1})$ and $v_g(\pm 1.8$ cm·s$^{-1})$. These values approach the value of 'uncertainty' in (u_g, v_g), which is estimated from the accuracy of individual data points in the pressure records.

4.2. WIND-DRIVEN MOTION; GLOBAL SOLUTION

From (6) time series are constructed by using the observed wind stress and the bottom profile. Using the parameters r, t and L as adjustable parameters, the ranges for finding a best-fit between these time series and the data in terms of the lowest 'error s.d.' are: $0.5 \cdot 10^{-3} < r < 1.5 \cdot 10^{-3}$ m s^{-1}, $0 < t < 36$ h (in 6-h units) and 230 km (excluding Dogger Bank) $< L <$ 315 km (including Dogger Bank). Sometimes appreciably better fits are obtained for (large) values of r (up to $r = 5 \cdot 10^{-3}$ m s^{-1}). In these model cases of large r, the wind stress curl term in (6) is small and (6) expresses balance between wind- and bottom stress. The wind stress curl term is more or less equally important as the along-isobath wind stress term in (6) during periods of largest observed currents, *e.g.* between days 156-159 in 1986 (Fig. 11; see also Fig. 3). Visually (Fig. 11) the model seems in better agreement with the observations than may be concluded from the 'error s.d.'s', which are near 75% of the s.d.'s of the data series (Table 3). Part of the large 'error s.d.' is due to time shifts which are masked when a visual comparison is made. Generally the time needed for the current to be established is small ($t \approx 6$ h).

The importance of continuous knowledge of the amount of stratification and of the proper vertically integrated current becomes clearer when time series based on (6) are fitted with the data for short periods of 5–10 days, notably for periods during which a large along-isobath current is observed. For these periods the s.d. of the 'error' series is near 50% of the s.d. of the observed series. Note, in Table 3, the large time-lag of 30 h needed for obtaining the best-fit for day 152–160 1986 and a relatively large bottom friction velocity of $r = 3 \cdot 10^{-3}$ m s^{-1}.

Due to the large portion of the data that is unexplained by the model (6), it is impossible to subtract properly the vertically averaged wind-driven motion from the data. Thus in this way other flow aspects cannot be investigated from the remaining part of the data. Models describing these aspects are best compared with the current observations after subtraction of the geostrophically balanced part of the currents by using the pressure series observed at moorings B and F.

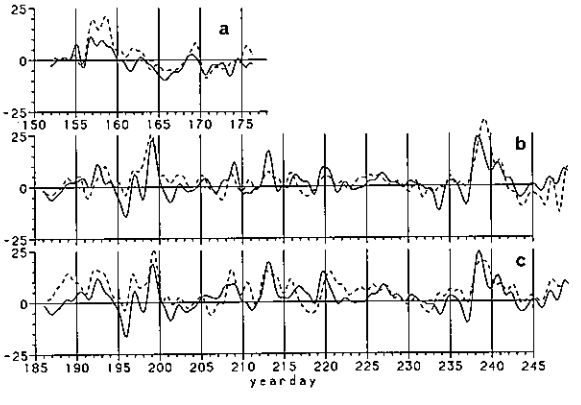

Fig. 11. Comparison between time series of the along-isobath current component obtained from the 'global' wind-driven model (6) (——) and from observations (----). The best-fit parameters are given in Table 3. The unit of the vertical axis is cm·s^{-1}. a. June 1986, observations from mooring B. b. July/August 1987, observations from mooring B. c. July/August 1987, observations from mooring A.

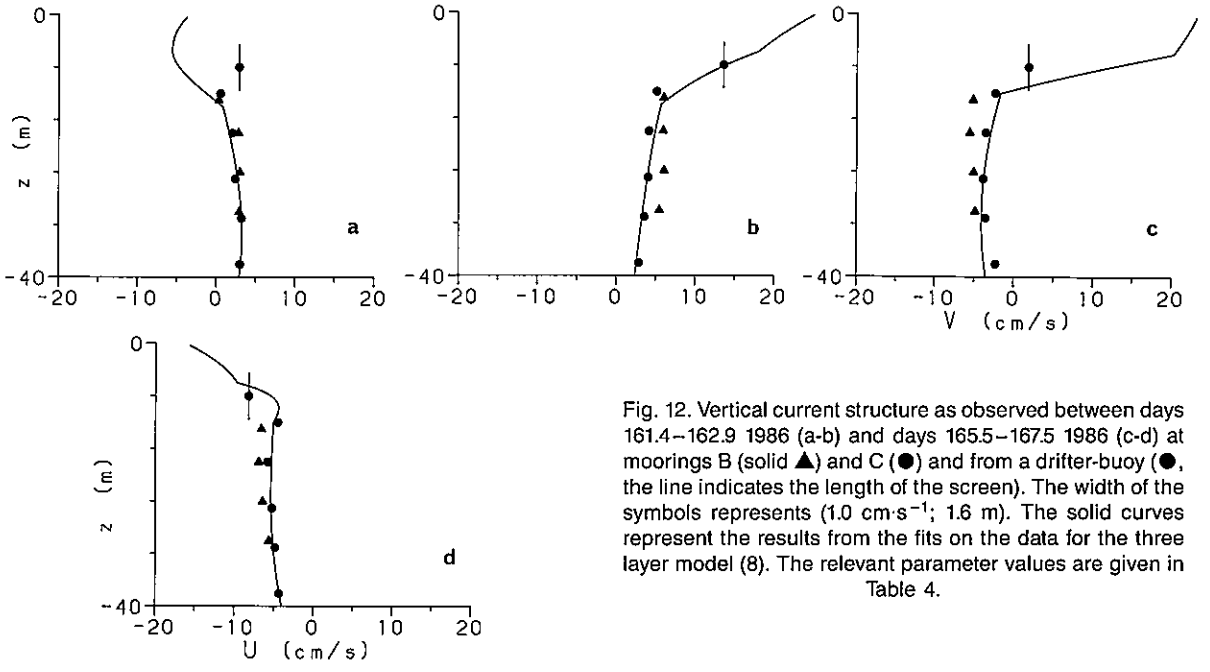

Fig. 12. Vertical current structure as observed between days 161.4–162.9 1986 (a-b) and days 165.5–167.5 1986 (c-d) at moorings B (solid ▲) and C (●) and from a drifter-buoy (●, the line indicates the length of the screen). The width of the symbols represents (1.0 cm·s^{-1}; 1.6 m). The solid curves represent the results from the fits on the data for the three layer model (8). The relevant parameter values are given in Table 4.

4.3. WIND-DRIVEN MOTION; LOCAL SOLUTION

Model (8) is verified with data from moorings B and C averaged over the periods 161.4–162.9 and 165.5–167.5 in 1986. With the estimates of h_1 and h_2 from the density distributions (Fig. 5c-d), only K_2 is unknown and therefore kept as an adjustable variable. The values $r=1.0\cdot10^{-3}$ m s^{-1}, $h_1=6$ m and $h_2=14$ m are kept constant. For K_3, only the values for the two limits described by CSANADY (1982) are chosen. Extra near-surface current estimates are obtained from a drifter buoy deployed for periods of 1–3 days and actually used for different experiments (Westra, pers. comm.).

TABLE 4

Comparison of the vertically averaged current (U_o,V_o), observed at moorings B and C, with results from the three-layer model (8). From the model vertical averages are calculated from surface to bottom ($_t$) and from 10 m depth to the bottom ($_p$). The geostrophic current components u_g,v_g are obtained from pressure gauges (^{m}), but they are sometimes changed to obtain a better fit with the data (^{u}). The units are cm·s^{-1} for the currents and $\cdot10^{-3}$ m^{2}s^{-1} for K_2, K_3.

	161.4-162.9 1986 $K_1=11.1\cdot10^{-3}$ *m²s⁻¹*	*165.5-167.5 1986* $K_1=13.4\cdot10^{-3}$ *m²s⁻¹*
Fig. 12:	a - b	c - d
input:		
u_g^m, u_g^u:	6.0, 6.5	−7.0, −8.0
v_g^m, v_g^u:	2.7, 3.5	−0.5, −2.0
K_2, K_3:	5.0, 25.0	2.0, 25.0
output:		
U_t, U_p:	7.9, 4.4	−6.2, −5.0
V_t, V_p:	0.4, 2.1	2.0, −3.2
U_o, V_o:	B:6.0,2.4 C:4.0,2.4	B: −6.5, −5.2 C: −5.1, −3.4

Model (8) is verified with data from moorings B and C averaged over the periods 161.4–162.9 and 165.5–167.5 in 1986. With the estimates of h_1 and h_2 from the density distributions (Fig. 5c-d), only K_2 is unknown and therefore kept as an adjustable variable. The values $r=1.0\cdot10^{-3}$ m s^{-1}, $h_1=6$ m and $h_2=14$ m are kept constant. For K_3, only the values for the two limits described by CSANADY (1982) are chosen. Extra near-surface current estimates are obtained from a drifter buoy deployed for periods of 1–3 days and actually used for different experiments (Westra, pers. comm.).

Fig. 12 and Table 4 show the model's results, which are obtained by minimizing the 'error' s.d. of the cross-isobath current component. The currents observed by means of the buoy are somewhat uncertain, because the attached 7-m-long screen is positioned between 4.5 and 11.5 m, *i.e.* generally in the highly sheared surface layer. Except for the v-component during the period 161.4–162.9, the values agree reasonably with the curves fitted on the current meter data. Between days 161.4–162.9 the density difference between surface and bottom amounts 0.25 kg m^{-3}, about two times weaker than between days 165.5–167.5. This probably explains why the best fitting profiles are obtained for higher values of K_2 during the first period ($K_2\approx0.2\cdot K_3$) compared to the second ($K_2\approx0.08\cdot K_3$).

Probably due to errors in the pressure series some values of the geostrophic current had to be changed to obtain a better fit between the model and the data. Another possible explanation for the observed, somewhat larger magnitudes of the vertically constant currents is indicated by CSANADY (1982). His model for wind-driven motion in a homogeneous sea of constant depth indicates a geostrophic current which decreases exponentially seaward in magnitude at a rate of the external Rossby radius, predicting a 20% magnitude difference between moorings B and F. However, the changes are still within the error bounds given in Section 4.1.

The agreement between the curves and the data

found for the shallow water limit $K_3^{(1)}$ is slightly better than for $K_3^{(2)}$. Probably in (10) the thickness of the bottom layer has to be taken instead of the total water depth, but even then $f(H-h_2)/u_* \approx 0.2$, which is larger than the limit given by CSANADY (1982).

Values of the vertically averaged currents are obtained from the profiles in Fig. 12 by averaging from surface to the bottom, $(U,V)_t$, and by averaging from 10 m depth to the bottom, $(U,V)_p$. The latter gives values comparable to the values from current meter observations. The partly vertically averaged U_p is about 2/3 of the totally vertically averaged U_t. For the v-component the former type of average is two times larger and sometimes opposite in sign, when compared with the total averages which generally are close to 0 (Table 4). Clearly the model indicates that under stratified conditions a large error is introduced by using V_p instead of V_t. Although this indicates

TABLE 5

Comparison between observed currents (u,v) averaged over typically 2-3 days with the barotropic geostrophic currents obtained from pressure observations at moorings B and F (u_g,v_g) and the density driven currents resulting from the models (12), (13) and (14) for several periods in 1986. For model (12) four different results are presented:for 'shallow' (s) and 'deep' (d) water limits, both without and including (T) wind stress (see text). The unit is cm·s^{-1} for the currents and m for the depths of the current meters.

period: 152.0-154.5		τ_x=0.01 N m^{-2}; τ_y=0.03 N m^{-2}						
mooring	u	u_g	u_{12s}	u_{12sT}	u_{12d}	u_{12dT}	u_{13}	u_{14}
A 14	4.5	1.2	2.7	3.6	4.1	4.0	3.9	−0.9
20	6.5	1.2	3.5	4.2	4.3	4.1	4.3	−0.6
25	6.7	1.2	3.8	4.3	4.0	3.9	4.5	−0.3
mooring	v	v_g	v_{12s}	v_{12sT}	v_{12d}	v_{12dT}	v_{13}	v_{14}
A 14	2.7	1.5	5.2	4.9	2.4	1.8	2.2	−0.2
20	4.0	1.5	4.9	4.5	2.7	2.6	2.3	−0.2
25	4.9	1.5	4.4	4.0	3.0	3.0	2.4	−0.1
period: 161.4−162.9		τ_x=0.21 N m^{-2}; τ_y=0.03 N m^{-2}						
mooring	u	u_g	u_{12s}	u_{12sT}	u_{12d}	u_{12dT}	u_{13}	u_{14}
A 14	11.2	6.0	7.8	12.9	9.6	6.3	9.1	−3.4
25	12.3	6.0	9.1	10.7	10.2	9.7	11.5	−1.1
mooring	v	v_g	v_{12s}	v_{12sT}	v_{12d}	v_{12dT}	v_{13}	v_{14}
A 14	0.0	2.7	7.2	0.9	3.8	0.2	3.6	−0.9
25	7.3	2.7	6.8	1.4	5.9	6.8	4.2	−0.3
period: 163.0−165.0		τ_x=−0.01 N m^{-2}; τ_y=0.03 N m^{-2}						
mooring	u	u_g	u_{12s}	u_{12sT}	u_{12d}	u_{12dT}	u_{13}	u_{14}
A 14	−3.7	−4.6	−2.3	−1.4	−2.9	−2.6	−2.9	−3.2
25	−1.9	−4.6	0.5	1.2	−0.9	−1.0	−1.2	−0.7
mooring	v	v_g	v_{12s}	v_{12sT}	v_{12d}	v_{12dT}	v_{13}	v_{14}
A 14	−4.2	−2.0	−2.7	−2.4	−1.6	−2.1	−1.5	−0.6
25	0.9	−2.0	−1.9	−2.0	−1.4	−1.4	−1.1	−0.2
period: 165.5−167.5		τ_x=−0.24 N m^{-2}; τ_y=0.05 N m^{-2}						
mooring	u	u_g	u_{12s}	u_{12sT}	u_{12d}	u_{12dT}	u_{13}	u_{14}
A 14	−9.7	−7.0	−9.2	−8.0	−12.5	− 7.8	−11.9	0.3
25	−7.5	−7.0	−6.9	−4.1	−10.5	−10.8	−11.6	0.3
mooring	v	v_g	v_{12s}	v_{12sT}	v_{12d}	v_{12dT}	v_{13}	v_{14}
A 14	−3.2	−0.5	−10.9	−3.4	−2.1	−2.0	−1.8	0.1
25	−0.5	−0.5	− 9.0	−4.5	−4.1	−5.0	−1.8	0.1

COMPARISON OF OBSERVATIONS AND MODELS AVERAGED OVER THE PERIODS GIVEN ABOVE

mooring	$u-u_{12s}$	$u-u_{12sT}$	$u-u_{12d}$	$u-u_{12dT}$	$u-u_{13}$
A 14	0.8±1.9	−1.2±1.2	1.0±1.3	1±3	1.0±1.2
25	1±2	−1±3	1.7±1.6	2.0±1.7	1.6±1.8
mooring	$v-v_{12s}$	$v-v_{12sT}$	$v-v_{12d}$	$v-v_{12dT}$	$v-v_{13}$
A 14	−1±5	−1.2±0.9	−1.8±1.5	−0.7±1.1	−1.8±1.5
25	3±3	3.4±1.8	2.3±0.8	2.3±1.4	2.2±0.7

that in (6) $(U,V)_t$ should be used, uncertainties of the time evolution of the stratification, on which the magnitude of the vertically averaged current depends, do not allow for the introduction of a time series of $(U,V)_t$.

4.4. DENSITY-DRIVEN MOTION

The currents observed during the sub-periods in June 1986, which are shown in Fig. 5, are compared with the models (12)-(14) for mooring A (Table 5). The accuracy of the density observed by a Neil Brown smart CTD amounts ≈ 0.01 kg m^{-3}, which results in an uncertainty in observed density differences of ± 0.015 kg m^{-3}. The time necessary for the ship to pass a frontal zone near mooring A was 1 h; during the periods to be discussed in this section a front is passed several times. Between two passages the stability of the position of a front is not known. Averaging the data from two passages along the same track, an average additional uncertainty of ± 0.04 kg m^{-3} is estimated. Then, with an average distance of 8 km between the CTD stations, the estimated maximum uncertainty in the density-induced current amounts ± 1.7 cm·s^{-1}. Including the uncertainty in the geostrophic current (Section 4.1.) an uncertainty of ± 3 cm·s^{-1} is expected for the currents which result from the models (12)-(14).

In (12) two adjustable parameters $K(=K_3)$ and r are apparent. Values for two limits are used: for a 'shallow-water' limit: $K=25\cdot10^{-3}$ m^2 s^{-1}, $r=1.0\cdot10^{-3}$ m s^{-1} (best-fit in Section 4.3) and for a 'deep-water' limit: $K=2.3\cdot10^{-3}$ m^2 s^{-1}, $r=0.3\cdot10^{-3}$ m s^{-1}.

Except perhaps for the period between days 163–165, (14) does not explain the currents observed (Table 5). It is not clear why a compensation of the density-induced pressure gradient by an adjustment of the sea level is absent near mooring A. Probably the time needed for the installment of this adjustment is considerably larger than the variation in time of the density field. Model (13) considerably better explains the currents observed. Depending on the period that is considered, only slightly further improvement is obtained by taking into account internal friction, *i.e.* by using (12) with $T=0$ (no wind stress). For the two periods with considerable wind stress the agreement of (12) with the observations is again slightly improved when $T\neq 0$ is taken.

Despite the large uncertainties, a distinct part of the observed currents remains unexplained (Table 5). The misfits between (12), (13) and the data observed at A are remarkably uniform, however. From Table 5 we find for model (13) at 14 m: u-$u_{13}=1.0\pm1.2$ cm·s^{-1}, v-$v_{13}=-1.8\pm1.5$ cm·s^{-1} and at 25 m: u-$u_{13}=1.6\pm1.8$ cm·s^{-1}, v-$v_{13}=2.2\pm0.7$ cm·s^{-1}. The uncertainties given here are determined by averaging the misfits between (13) and the data of all four periods in Table 5. They are on average half of the uncertainty estimated at the beginning of this section (± 3 cm·s^{-1}). Especially at 25 m the values given above still correspond with the excess current observed at A (Section 2). The average residual vertical shear of $\Delta v/\Delta z \approx -0.35\ 10^{-2}$ s^{-1} is equivalent to the persistent shear shown in Fig. 7. An explanation will be suggested in the next section in which stratification in the frontal zone is important.

TABLE 6

In- and output parameter values for the non-linear tide-topography interaction model developed by MAAS & ZIMMERMAN (1989). See text for explanation of the symbols. Some observed parameter values are included.

	model	*observed*
input:		
A (m s^{-1})	0.25	0.15(M_2);0.25(total tidal current)
l_0 (km)	1.8	
$\partial H/\partial y$ ($\cdot10^{-3}$)	1.5	1.2
l_t (km)	2.3	
$\Delta\varrho$ (kg m^{-3})	1.0	<1.0
l_i (km)	4.8	
output:		
u_{max}(cm·s^{-1})	2.6	
Ψ_{min}(m^{2}s^{-1})	−0.026	
ψ_{max}(m^{2}s^{-1})	0.088	

4.5. NON-LINEAR TIDE-TOPOGRAPHY INTERACTION

Considering linearly stratified fluids MAAS & ZIMMERMAN (1989) describe the residual response for tidal interaction with a small amplitude arctangent-shaped topography under weakly damped conditions. Under these conditions only bottom friction is considered: $r = E_-^{0.5}$. $E_-=2K/(\sigma H^2(1-f))$ denotes the Ekman-Stokes number due to the anticyclonically rotating current component in which f is scaled with σ, the tidal frequency. MAAS (1987) indicates, but does not present, solutions under strongly damped conditions, when the fluid may be interpreted as a two-layer system, which is actually more realistic for our purposes. Therefore quantitatively the influence of strong damping is unknown.

The relevant parameters are the length scale of the bottom topography (l_t), the tidal excursion amplitude (l_0) and the cross-isobath tidal current amplitude (A_{M2}). Due to the stratification an extra length scale, the internal Rossby radius $l_i=NH/f$, is introduced, in which $N^2=-g\Delta\varrho/\varrho H$ denotes the Brunt-Väisälä frequency.

The spectral representation of the result for the rectified along-isobath current and the cross-isobath streamfunction reads:

$$u_k = -ikfH_k \frac{k'}{\sinh(k')} \cosh(k'z) \cdot \left(\frac{1-J_0^2(k)}{k^2}\right)$$

$$\psi_k = -ikrH_k \frac{k'}{\tanh(k')} \left[z \cdot \frac{\cosh(k'z)}{\cosh(k')} - \frac{\sinh(k'z)}{\sinh(k')}\right] \cdot \left(\frac{1-J_0^2(k)}{k^2}\right) \quad (17)$$

in which all variables are dimensionless, the sub-index k denotes the spectral representation and $i = \sqrt{-1}$. J_0 is a Bessel function of zeroth order, k the topographic wave number (scaled with l_0) and k' the internal wave number (scaled with l_i). $H_k = iH'/2k \cdot \exp(-|k| l_i/l_0)$ denotes the spectral topography, which represents the spectral image of an arctangent-shaped bottom topography with H' the non-dimensional topographic amplitude in real space (scaled with H).

The spectral solutions (17) consist of three factors: one related to the topography spectrum (by H_k), the second is a stratification function dependent on depth (z) and internal wave number (k') and finally the influence of quasi-nonlinear advection which depends on the topographic wave number k. To obtain the dynamic field variables (u and ψ) in real space, an inverse Fourier transform of (17) has to be calculated, which, however, exists analytically for a step-topography only. Here the inverse Fourier transform is calculated numerically with parameter values appropriate for our conditions.

The numerically obtained results are dimensionalized. The relevant parameter values are given in Table 6. All length scales are a little over-estimated to obtain a better fit with the data. The results, visualized in Fig. 13 for the along-isobath current and in Fig. 14c for the cross-isobath component, show enhanced current components near the bottom and a three cell cross-isobath circulation due to the squeezing of vortex tubes by the stratification.

The model explains quantitatively the residual currents at mooring A. However, the model shows that this result is strongly dependent on the exact position of A in relation to the steepest bottom slope, even more so when the tidal excursion is smaller.

The result is parametrically dependent on the slow evolution of the stratification above the bottom slope. The along-isobath rectified current component will however always be directed with the shallow water at its right-hand side. As the density stratification is approximately determined in half by temperature, the topographically rectified current is at least expected

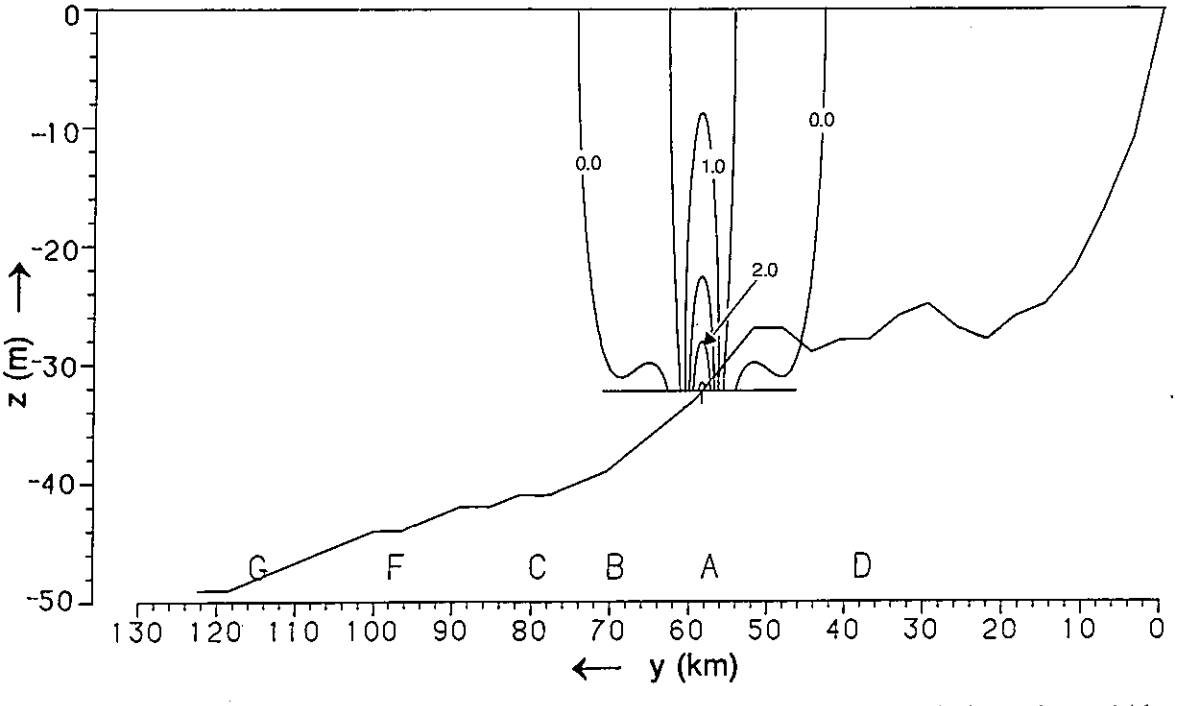

Fig. 13. Contours of constant along-isobath velocity as derived from the non-linear tide-topography interaction model for a small-amplitude topography in a linearly stratified fluid as developed by MAAS & ZIMMERMAN (1989). The relevant parameters are given in Table 6. The unit is cm·s^{-1}.

to appear from day 165–175 in 1986 and from day 186–195 in 1987 (Fig. 3f). An intensified along-isobath current component near mooring F for example cannot be explained by this rectifying mechanism, because the bottom slope is too small ($\approx 0.3 \cdot 10^{-3}$).

Assuming that the conditions under which the model is applied are valid for all periods in 1986 shown in Table 5, the rectified current values (u_r,v_r) at both current-meter depths of mooring A are: at 14 m: u_r=1.2 cm·s^{-1}, v_r=−0.4 cm·s^{-1} and at 25 m: u_r=1.8 cm·s^{-1}, v_r=1.5 cm·s^{-1}. These values correspond with the unexplained part which remained at the end of Section 4.4. One should note, however, the large uncertainties in the geostrophic current and the density-induced current and the assumptions made in this section.

5. CIRCULATION IN THE CROSS-ISOBATH (Y-Z) PLANE

The wind-driven circulation for a positively directed along-isobath wind stress consists of a surface Ekman transport directed towards the coast and, due to the coastal boundary condition, of an offshore-directed adjustment drift near the bottom (Fig. 14a). As pointed out by CSANADY (1982) and LODER & WRIGHT (1985) the width of the highly frictional coastal (shallow-water) boundary layer (c.b.l.) is uncertain. In their near-coastal model MITCHUM & CLARKE (1986) assume that the c.b.l. (in which the surface and bottom Ekman layers interact) reaches towards a position with a water depth of three times the frictional Ekman depth, *i.e.* 30–45 m under moderate wind conditions ($|\vec{\tau}|$=0.15–0.3 N m^{-2}). CSANADY (1982) shows that streamlines, which describe wind-driven motion in a vertical plane perpendicular to the coast, close in the c.b.l.

The water masses transported by the mean residual currents from the Channel and the English coast (PRANDLE, 1984) converge near A, thereby developing a frontal zone. The dominating role of internal friction in cross-frontal circulation is acknowledged by MOOERS *et al.* (1978) and GARRETT & LODER (1981). Due to horizontal and vertical geostrophic current shear, an Ekman layer is thought to establish on both

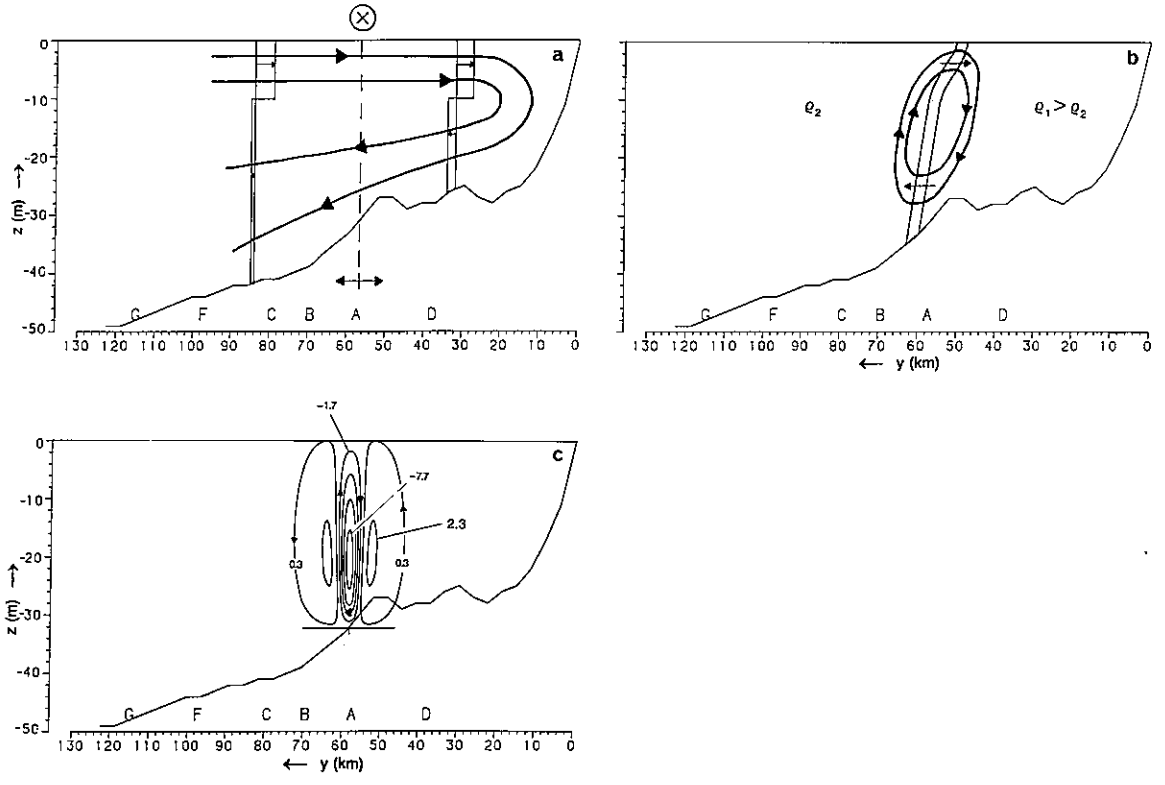

Fig. 14. Streamline patterns (solid curves) from models in the y-z plane. a. Wind-driven circulation for positively directed along-isobath wind stress. The arrows and rectangles show the inferred cross-isobath current component. The vertical dashed line represents the border of the coastal boundary layer, of which the position is dependent on the wind stress magnitude (see text). b. Differential advection (arrows) and density-induced circulation (after GARRETT & LODER, 1981). c. Nonlinear tide-topography interaction induced rectified circulation of the model developed by MAAS & ZIMMERMAN (1989). The unit is $\cdot 10^{-2}$ m^{2}s^{-1}.

sides of the front. In these layers the Ekman fluxes have opposite signs. If surface and bottom Ekman layers are included, a one-cell circulation develops for the front depicted in Fig. 14b. Due to differential advection in the vertical by the wind-induced transport, the front is twisted, thereby initiating stratification (Fig. 14b; VAN AKEN, 1986).

When stratification has been established a circulation pattern due to non-linear tide-topography interaction may develop (Fig. 14c). The result depicted in Fig. 14c has been calculated without consideration of the higher order interactions. TEE (1985) and LODER & WRIGHT (1985) have shown that these may cause the centre cell to move towards the crest of the slope and the left (weak) cell to broaden.

All proposed circulation patterns appear to reinforce each other near mooring A when:

1. the wind stress is moderate ($|\vec{\tau}| \approx 0.2$ N m^{-2}) and directed positively along-isobath (*i.e.* for westerly winds) and when
2. two water masses, the densest one coming from the Channel, generate an oblique frontal zone such that:
3. stratification develops at the same location.

From the observed distribution of the cross-isobath current component $v(y,z)$ a streamline pattern $\psi(y,z)$ is inferred such that $\partial\psi/\partial z = -v$ and $\partial\psi/\partial y = w$. This definition of the stream function is valid only if the

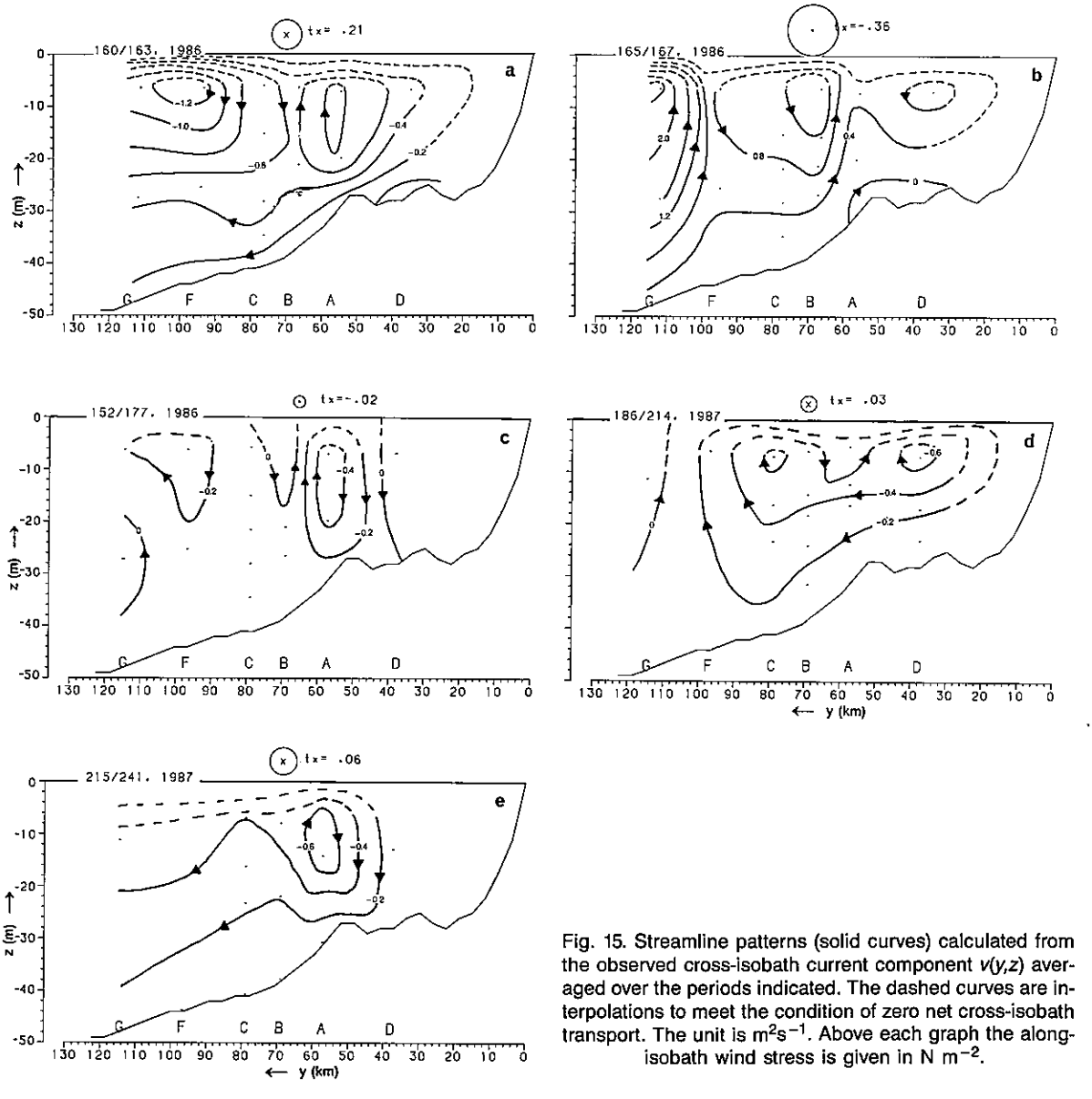

Fig. 15. Streamline patterns (solid curves) calculated from the observed cross-isobath current component $v(y,z)$ averaged over the periods indicated. The dashed curves are interpolations to meet the condition of zero net cross-isobath transport. The unit is m^{2}s^{-1}. Above each graph the along-isobath wind stress is given in N m^{-2}.

divergence in the along-isobath direction ($\partial u/\partial x$) can be neglected (Section 2.2). Using as a boundary condition that the current perpendicular to the bottom vanishes at $z=-H$, ψ is calculated for each mooring by integrating the observed v from the bottom to 10 m depth. Examples of the interpolated streamline pattern are shown in Fig. 15, in which the dashed lines in the upper layer have been drawn to guarantee that there is no net cross-isobath transport. Fig. 15 has been derived from and is to be compared with Figs 4 and 5.

Focussing on the circulation pattern near mooring A in Fig. 15a, we observe a reinforcement of the three models. A comparison of Fig. 15a and Fig. 15b shows a different circulation in Fig. 15b with dominating (reversed) wind- and density-induced circulations and a weak influence of the rectified circulation, which is still observable near the bottom by the enhanced upwelling between A and B. Generally the observed circulation is mirrored in the density distribution as the upwelling zones in the streamline pattern more or less agree with a tilting of the isopycnals (compare Fig. 15a-b with 5c-d).

Considering the monthly averages, June 1986 and August 1987 (Fig. 15c and 15e) show similar but weaker patterns than in Fig. 15a. Probably the non-zero positive along-isobath wind stress dominates the pattern in July and August 1987, whereas the rectified circulation explains the period of June 1986. However, the magnitude of the circulation created by the tide-topography interaction (Fig. 14c) is about three times weaker than found in Fig. 15c. An estimate of the monthly averaged density circulation cannot be given.

An example of poor qualitative agreement between the models and the data is found in Fig. 15a-b near the moorings F and G. In these figures the general wind-induced circulation is easily detected, but two reinforcing circulation cells, equal in sign, border each other, suggesting a saddle point near C. Because of the density distributions in Fig. 5c a circulation cell opposite in sign to the wind-driven circulation is expected near F, which is not observed. The v-component observed at F and G acts as if the c.b.l. borders these moorings, because they show an enhanced 'wind-driven' circulation. More likely, the number of current meters at these moorings is too small for a construction of the stream function.

6. CONCLUSIONS

The sub-tidal currents are predominantly wind-driven. Quantitatively the 'global' wind-driven model and the observations differ considerably when the total periods of measurements are considered. This is mainly due to the poor determination of the vertically averaged current and to the (unknown) space and time variability of the stratification rate (Sections 4.1 and 4.2).

The area above the steepest bottom slope near mooring A shows two important dynamical aspects in addition to wind forcing. This area coincides with the transition between stratified and well-mixed waters, but the density-induced pressure gradient inferred does not obey the thermal wind relation when applied with a bottom boundary condition. To a fair approximation, the density-driven motion is described by calculating solutions of the same relation relative to the surface. A model on density-driven motion which accounts for internal friction explains the observations only slightly better than the latter model. Additionally a distinct part of the near-bottom intensified along-isobath current component and the off-slope cross-isobath current component point to the non-linear tide-topography interaction mechanism.

Noting the uncertainty bounds given in Section 4, the current at mooring A has been reconstructed quantitatively for the period between days 161.4–162.9. For the near-bottom along-isobath current component 6 ± 2 cm/s is due to the wind-induced barotropic pressure gradient, 5.5 ± 1.7 cm/s to the quasi-permanent front and 1.8 cm/s to the rectifying mechanism. The magnitude of the observed along-isobath current component is 12.3 cm/s. For the near-bottom cross-isobath current component these values are: 2.7 ± 1.8, 2.6 ± 1.7, 1.5 and 7.3 cm/s. For all other moorings only a wind-induced current is found, except during the passage of a front.

Assuming the combined density- and tide-topography-induced circulation cell near A to be 10 km wide, the turnover time for a particle travelling this cell is 11 days, provided the net cross-isobath transport equals zero. In this period the density and rectified parts of the along-isobath current component may have advected material from a distance of 55 km west of A. In contrast to these momentary values, the monthly averaged values read 16 days and 40 km, respectively.

Future experiments on the subject treated in this text should be performed with current meters closer to the surface or with moored ADCP and with moorings located over a bottom slope at shorter mutual distances than used here. Preferably are also the use of ship-mounted or -towed equipment such as ADCP and Batfish, which provide high resolution spatial distributions of current and hydrography, respectively. Then, better estimates may be obtained of the 'global' wind-driven solution and of the tide-topography interaction.

7. REFERENCES

AKEN, H.M. VAN, 1986. The onset of seasonal stratification in shelf seas due to differential advection in the presence of a salinity gradient.—Cont. Shelf Res. **5:** 475-485.

AKEN, H.M. VAN, G.J.F. VAN HEIJST & L.R.M. MAAS, 1987. Observations of fronts in the North Sea.—J. Mar. Res. **45:** 579-600.

BOWDEN, K.F., 1953. Note on wind drift in a channel in the presence of tidal currents.—Proc. Roy. Soc. **A219:** 426-446.

——, 1983. Physical oceanography of coastal waters. Ellis Horwood Ltd., Chichester: 1-302.

BUTMAN, B. & R.C. BEARDSLEY, 1987. Long-term observations on the southern flank of Georges Bank. Part I: a description of the seasonal cycle of currents, temperature, stratification and wind stress.—J. Phys. Ocean. **17:** 367-384.

CSANADY, G.T., 1982. Circulation in the coastal ocean. Reidel Publishing Company, Dordrecht: 1-279.

GARRETT, C.J.R. & J.W. LODER, 1981. Dynamical aspects of shallow sea fronts.—Phil. Trans. R. Soc. Lond. **A302:** 563-581.

HAREN, J.J.M. VAN, 1990. Sub-tidal dynamics of a near-coastal zone in the North Sea.—Neth. J. Sea Res. **25:** 31-44.

LEE, A.J., 1980. North Sea: physical oceanography. In: F.T. BANNER, M.B. COLLINS & K.S. MASSIE. The North-West European Shelf seas: the sea bed and the sea in motion. II. Physical and chemical oceanography, and physical resources. Elsevier Scientific Publishing Company, Amsterdam: 467-493.

LI, H., J.J.M. VAN HAREN & H.M. VAN AKEN, 1989. Cluster analysis as a method to discriminate water masses in shelf seas. ICES-paper Hydography Committee C.M. 1989/C:3: 1-14.

LODER, J.W., 1980. Topographic rectification of tidal currents on the sides of Georges Bank.—J. Phys. Ocean. **10:** 1399-1416.

LODER, J.W. & D.G. WRIGHT, 1985. Tidal rectification and frontal circulation on the sides of Georges Bank.—J. Mar. Res. **43:** 581-604.

MAAS, L.R.M., 1987. Tide-topography interactions in a stratified shelf sea. Ph.D. thesis, Univ. Utrecht: 1-241.

MAAS, L.R.M. & J.J.M. VAN HAREN, 1987. Observations on the vertical structure of tidal and inertial currents in the central North Sea.—J. Mar. Res. **45:** 293-318.

MAAS, L.R.M., J.T.F. ZIMMERMAN & N.M. TEMME, 1987. On the exact shape of the horizontal profile of a topographically rectified tidal flow.—Geophys. Astrophys. Fluid Dyn. **38:** 105-129.

MAAS, L.R.M. & J.T.F. ZIMMERMAN, 1989. Tide-topography interactions in a stratified shelf sea II. Bottom trapped internal tides and baroclinic residual currents.—Geophys. Astrophys. Fluid Dyn. **45:** 37-69.

MITCHUM, G.T. & A.J. CLARKE, 1986. The frictional nearshore response to forcing by synoptic scale winds.—J. Phys. Ocean. **16:** 934-946.

MOOERS, C.N.K., C.N. FLAGG & W.C. BOICOURT, 1978. Prograde and retrograde fronts. In: M.J. BOWMAN & W.E. ESAIAS. Oceanic fronts in coastal processes. Springer-Verlag, Berlin: 43-58.

NOBLE, M., B. BUTMAN & E. WILLIAMS, 1983. On the long-shelf structure and dynamics of subtidal currents on the Eastern United States Continental Shelf.—J. Phys. Ocean. **13:** 2125-2147.

PINGREE, R.D. & D.K. GRIFFITHS, 1978. Tidal fronts on the shelf seas around the British Isles.—J. Geophys. Res. **83:** 4615-4622.

POND, S. & G.L. PICKARD, 1986. Introductory dynamical oceanography. Pergamon Press, Oxford: 1-329.

PRANDLE, D., 1984. A modelling study of the mixing of ^{137}Cs in the seas of the European Continental Shelf.—Phil. Trans. R. Soc. Lond. **A310:** 407-436.

SIMONS, T.J., 1980. Circulation models of lakes and inland seas.—Can. Bull. Fish. Aquat. Sci. **203:** 1-146.

TEE, K.-T., 1985. Depth-dependent studies of tidally induced residual currents on the sides of Georges Bank.—J. Phys. Ocean. **15:** 1818-1846.

WEENINK, M.P.H., 1958. A theory and method of calculation of wind effects on sea levels in a partly-enclosed sea, with special application to the southern coast of the North Sea. KNMI-mededelingen en verhandelingen no 73. 1-111.

ZIMMERMAN, J.T.F., 1978. Topographic generation of residual circulation by oscillatory (tidal) currents.—Geophys. Astrophys Fluid Dyn. **11:** 35-47.

——, 1980. Vorticity transfer by tidal currents over an irregular topography.—J. Mar. Res. **38:** 601-630.

(received 20 February 1990; revised 10 August 1990)